# Fault diagnosis of a simulated model of an industrial gas turbine prototype using identification techniques

S. Simani[†], C. Fantuzzi[†], Ron J. Patton[‡]

[†]Dipartimento di Ingegneria
Università di Ferrara
Via Saragat, 1, 44100 Ferrara - Italy.
E-mail: ssimani@ing.unife.it

[‡]Faculty of Engineering & Mathematics, School of Engineering
Cottingham Road. Hull HU6 7RX, United Kingdom
E-mail: r.j.patton@eng.hull.ac.uk

February 11, 2000

**Abstract**

In this report a model-based procedure exploiting analytical redundancy for the detection and isolation of faults in a dynamic system is presented.

Despite the model complexity of the plant under observation, the report shows how simple linear models obtained from black box identification procedures can be effectively used to solve fault detection and identification problems.

Depending on signal to noise ratio, linear ARX or EIV models are identified in correspondence to some operating points of the plant. Fault detection of actuators, plant components and sensors are obtained through observer residual analysis, whilst statistical tests and signal processing based on multi-layer perceptron neural network are used to determine fault origins.

The report focuses on the application of the whole procedure, from system identification to residual analysis, to a prototype of a real single-shaft industrial gas turbine. Several fault causes are simulated using Matlab-Simulink software environment, aiming to test the proposed procedure. The most significance results from the massive tests performed are then reported and deeply discussed.

## 1 Introduction

The control devices which are nowadays exploited to improve the overall performance of industrial processes involve both sophisticated digital system design techniques and complex hardware (input-output sensors, actuators, components and processing units). Such a complexity results in an increased probability of failure occurrence. As a direct consequence of this, control systems must include automatic supervision of the closed-loop operation to detect and isolate malfunctions as early as possible.

The problem of fault detection and isolation (FDI) in linear time-invariant dynamic processes has received great attention during the last two decades and a wide variety of model-based approaches has been proposed [Isermann and Ballé, 1997, Chen and Patton, 1999].

These different methods, however, can be brought down to a few basic concepts such as the parity space approach [Gertler, 1998], the state estimation approach [Willsky, 1976, Isermann, 1984, Baseville, 1988, Frank, 1990, Xie et al., 1994, Xie and Soh, 1994], the fault detection filter approach [Frank, 1990, Patton, 1996, Frank and Ding, 1997] and the parameter identification approach [Willsky, 1976,

Baseville, 1988, Patton et al., 1989]. In every case, for the detectability and distinguishability of faults, mathematical models of the process under investigation are required, either in state space or input-output form.

State space descriptions provide general and mathematically rigorous tools for system modeling and residual generation which may be used in fault detection of industrial systems, both for the deterministic (noise-free case) and the stochastic (noisy case) environment. Residuals should then be processed to detect an actual fault condition, rejecting any false alarms caused by noise or spurious signals.

This report aims to define a comprehensive methodology for the diagnosis of actuator, component and input-output sensor fault of an industrial process by using an output estimation approach [Simani et al., 2000a], in conjunction with residual processing schemes which include a simple threshold detection, in deterministic case, as well as statistical analysis when data are affected by noise [Chen and Patton, 1999].

Two main aspects of the proposed methodology should be underlined.

Firstly, the FDI model-based approach does not require any physical knowledge of the process under observation. A linear mathematical model (state-space or input-output descriptions) of the input-output links are, in fact, obtained by means of identification schemes which use Auto Regressive eXogenous (ARX) models in case of high signal to noise ratios, or Errors-In-Variables (EIV) models, otherwise [Kalman, 1982, Kalman, 1990]. In the last case the identification technique is based on the Frisch scheme methodology [Frisch, 1934]. This approach gives a reliable model of the plant under investigation, as well as providing variances of the input-output noises [Beghelli et al., 1990].

Secondly, in this work linear prototypes for the design of linear output estimators [Simani et al., 1999a, Simani, 1999b], [Simani et al., 2000a] have been developed instead of complicated non-linear models obtained by modeling techniques in connection with non-linear observers. In fact, even if the number of studies addressing non-linear fault diagnosis theory steadily increases over the years, in some cases, linear approach still advantageous in terms of solution complexity and performance.

The complete procedure of model identification, residual generation and fault identification and isolation have been tested on a single-shaft industrial gas turbine prototype. The results coming from a massive simulation tests are reported and widely commented.

## 2 Plant model description

In the following it is assumed that the monitored system, depicted in Figure (1), can be described in fault free condition, by a linear, discrete-time, time-invariant, dynamic model of the type

$$\begin{cases} \mathbf{x}(t+1) &= \mathbf{A}\mathbf{x}(t) + \mathbf{B}\mathbf{u}^*(t) \\ \mathbf{y}^*(t) &= \mathbf{C}\mathbf{x}(t) \qquad\qquad t = 1, 2, \cdots \end{cases} \tag{1}$$

where $\mathbf{x}(t) \in \Re^n$ is the state vector, $\mathbf{y}^*(t) \in \Re^m$ the process output vector and $\mathbf{u}^* \in \Re^r$ the control input vector. $\mathbf{A}$, $\mathbf{B}$ and $\mathbf{C}$ are constant matrices of appropriate dimensions obtained by means of modeling techniques or identification procedures.

Under fault free conditions, the input and the output link of the sensors can be described by the following relation

$$\begin{cases} \mathbf{u}(t) &= \mathbf{u}^*(t) + \tilde{\mathbf{u}}(t), \\ \mathbf{y}(t) &= \mathbf{y}^*(t) + \tilde{\mathbf{y}}(t). \end{cases} \tag{2}$$

In real applications, variables $\tilde{\mathbf{u}}(t)$ and $\tilde{\mathbf{y}}(t)$ represent noises which, due to technological reasons, affect sensor behaviour. They are generally described as white, zero-mean, uncorrelated Gaussian noises. It is assumed that $\mathbf{u}(t)$ and $\mathbf{y}(t)$ are the only available measurements from the real process.

Vectors $\mathbf{f}_u(t) = \begin{bmatrix} f_{u_1} & \cdots & f_{u_r} \end{bmatrix}$ and $\mathbf{f}_y(t) = \begin{bmatrix} f_{y_1} & \cdots & f_{y_m} \end{bmatrix}$ model input and output sensor faults, respectively. The scheme shown in Figure (1) describes the relations among the actual sensor inputs $\mathbf{u}^*(t)$ and $\mathbf{y}^*(t)$, the sensor faults $\mathbf{f}_u(t)$ and $\mathbf{f}_y(t)$ and the sensor outputs $\mathbf{u}(t)$ and $\mathbf{y}(t)$.

According again to Figure (1), when a component fault $\mathbf{f}_s(t) \in \Re^n$ occurs in the plant described by Equations (1), the dynamic system will be modeled as

$$\mathbf{x}(t+1) = \mathbf{A}\mathbf{x}(t) + \mathbf{B}\mathbf{u}(t) + \mathbf{f}_s(t). \tag{3}$$

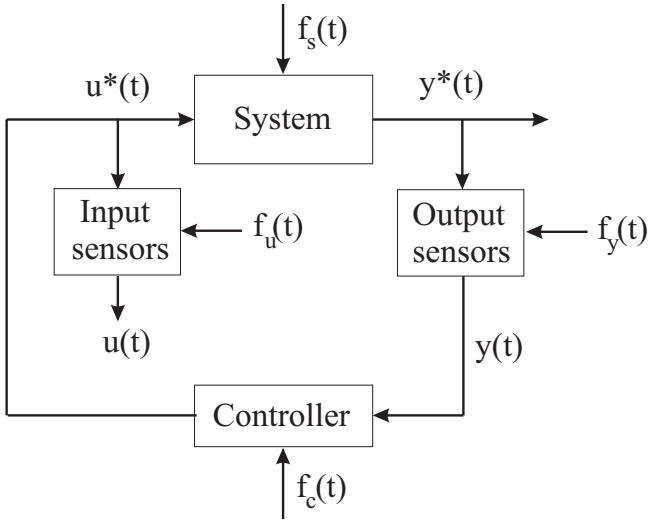


Figure 1: The monitored system

A fault $\mathbf{f}_c(t) = \mathbf{0}$ may also occur on the regulator in the control loop. In such a case, under the assumptions that $\mathbf{f}_u(t) = \mathbf{0}$ and $\mathbf{f}_y(t) = \mathbf{0}$, the link among the output $\mathbf{u}(t)$ of the regulator, its input $\mathbf{y}(t)$ and the controller fault $\mathbf{f}_c(t)$ will be modeled as

$$\mathbf{u}(t) = \tilde{\mathbf{u}}(t) + G\left(\mathbf{y}(\cdot)\right) + \mathbf{f}_c(t) \tag{4}$$

where $G(\cdot)$ represents the input-output behaviour of the controller.

Usually $\mathbf{f}_u(t)$, $\mathbf{f}_y(t)$, $\mathbf{f}_s(t)$ and $\mathbf{f}_c(t)$ signals are described by step and ramp functions representing abrupt and incipient faults (bias or drift), respectively.

Under fault-free assumptions, representations of types (1) and (2) are known as errors–in–variables (EIV) models.

The design of state observers and Kalman filters requires the knowledge of a state-space model of the system under investigation. When classical modeling techniques cannot be used since the complete physical knowledge of the system is not available or the model parameters are unknown, a black-box identification approach has to be considered.

# 3 Equation error models

In case of high signal to noise ratios ($\tilde{\mathbf{u}}(t) \cong \mathbf{0}$ and $\tilde{\mathbf{y}}(t) \cong \mathbf{0}$), equation error identification can be exploited and, in particular, different equation error models can be extracted from the data. A specific discrete-time, time-invariant, linear dynamic model, e.g. ARX or ARMAX (Auto Regressive eXogenous or Auto Regressive Moving Average eXogenous), [Leontaritis and Billings, 1985], can be selected only inside an assumed family of models.

If instead, the signal to noise ratios on the input and output of the process are low, the Frisch scheme [Frisch, 1934] can be applied to perform the dynamic system identification. Such a scheme allows to determine the linear discrete system which has generated the noisy sequences as well as the variances of the noises $\tilde{\mathbf{u}}(t) \cong \mathbf{0}$ and $\tilde{\mathbf{y}}(t) \cong \mathbf{0}$ affecting the data [Beghelli et al., 1990]. In the Frisch scheme these signals are assumed zero-mean white noises, mutually uncorrelated and uncorrelated with every component of $\mathbf{u}^*(t)$ and $\mathbf{y}^*(t)$.

In particular, in this work, the input-output link will be mathematically described by performing the identification of a number of ARX Multi-Input Single-Output (MISO) models of the type

$$y_i^*(t) = \sum_{j=1}^{n} \alpha_{i,j} y_i^*(t-j) + \sum_{j=1}^{r} \sum_{k=1}^{n} \beta_{i,j,k} u_j^*(t-k) + \varepsilon_i(t) \tag{5}$$

equal to the number $m$ of the output variables has been performed. The order $n$ and the parameters $\alpha_{i,j}$ and $\beta_{i,j,k}$, with $i = 1, \cdots, m$, of the model have to be determined by the identification approach. The term $\varepsilon_i(t)$ takes into account the modeling error, which is due to process noises, parameter variations, etc.

The next step is the transformation of input-output discrete-time time-invariant linear models (5) into state-space representations. The state-space systems obtained by the equation errors models are useful to design dynamic observers, whilst the ones coming from the Frisch scheme can be used in order to build Kalman filters.

It can be proved that a state-space formulation of the input-output equation error model (5) in fault free conditions, for the $i$-th output ($i = 1, \cdots, m$) becomes

$$\left\{ \begin{array}{lcll} \mathbf{x}_i(t+1) & = & \mathbf{A}_i \mathbf{x}_i(t) + \mathbf{B}_i \mathbf{u}^*(t) + \mathbf{B}_{\omega_i} \varepsilon_i & \\ \mathbf{y}_i^*(t) & = & \mathbf{C}_i \mathbf{x}_i(t) + \mathbf{D}_{\omega_i} \varepsilon_i, & t = 1, 2, \cdots \end{array} \right. \tag{6}$$

where the matrices $\mathbf{A}_i$ $(n \times n)$, $\mathbf{B}_i$ $(n \times r)$, $\mathbf{B}_{\omega_i}$ $(n \times 1)$, $\mathbf{C}_i$ $(1 \times n)$ and $\mathbf{D}_{\omega_i}$ are functions of the order and the $\alpha_{i,j}$ and $\beta_{i,j,k}$ parameters [Söderström and Stoica, 1987].

# 4 ARX model identification

Consider an assumed order for a SISO (Single-Input Single Output, $m = 1$) ARX model (5) and the input-output sequences $\{\mathbf{u}(t), \mathbf{y}(t)\}$ observed in the time interval $[1, L]$. If the model (5) is used to compute predicted output values $\mathbf{y}^*(t)$ in the $N = L - n$ times, for a given set of parameters

$$\theta = \left[ \begin{array}{cccccc} \alpha_n & \cdots & \alpha_1 & \beta_n & \cdots & \beta_1 \end{array} \right] \tag{7}$$

the mean square prediction error $J(\theta)$ is given by

$$J(\theta) = \frac{1}{N} \sum\nolimits_{t=n+1}^{L} \left( y^*(t) - y(t) \right)^2 . \tag{8}$$

By introducing now the following Hankel matrices $\mathbf{H}_u$ and $\mathbf{H}_y$

$$\mathbf{H}_n(u) = \left[ \begin{array}{ccc} u(1) & \cdots & u(n) \\ \vdots & \ddots & \vdots \\ u(L-n) & \cdots & u(L-1) \end{array} \right] \text{ and } \mathbf{H}_n(y) = \left[ \begin{array}{ccc} y(1) & \cdots & y(n) \\ \vdots & \ddots & \vdots \\ y(L-n) & \cdots & y(L-1) \end{array} \right], \tag{9}$$

it follows that

$$\left[ \begin{array}{c} y^*(n+1) \\ \vdots \\ y^*(L) \end{array} \right] = \left[ \mathbf{H}_n(y) \mathbf{H}_n(u) \right] \theta = \mathbf{H}_n \theta. \tag{10}$$

It can be proved that the parameter vector minimising the cost function (8) is given by

$$\hat{\theta} = \mathbf{H}_n^+ \left[ \begin{array}{c} y(n+1) \\ \vdots \\ y(L) \end{array} \right] = \mathbf{H}_n^+ y_n^o \tag{11}$$

where $\mathbf{H}_n^+$ denotes the pseudo-inverse of the $\mathbf{H}_n$ matrix. The algorithm gives an estimate $\hat{\theta}$ of $\theta$, which converges asymptotically to the real parameter of the process that has generated the data.

To estimate the order $n$ of the ARX process, an integer $k > 0$ and the $(N \times 2k + 1)$ matrix of input-output samples given by

$$\mathbf{H}_k^* = \left[ \mathbf{H}_k(y) \mathbf{H}_k(u) y_k^o \right] \tag{12}$$

are considered.

If $\varepsilon_i(t) = 0$ in (5) the following properties hold

$$\begin{array}{lcll} \text{rank}\,(\mathbf{H}_k^*) & = & 2k+1 & \text{for } 2k+1 < n \\ \text{rank}\,(\mathbf{H}_k^*) & = & 2k & \text{for } 2k \geq n \end{array} \tag{13}$$

It could be possible to consider the increasing sequence of matrices

$$\mathbf{S}_1 \ \mathbf{S}_2 \ \cdots \ \mathbf{S}_n \ \cdots \tag{14}$$

where $\mathbf{S}_k = \mathbf{H}_k^{*T}\mathbf{H}_k^*$ and to evaluate their singularity. The first singular matrix $\mathbf{S}_k$ would define the correct order for the model ($k = n$). Unfortunately, the presence of $\varepsilon_i(t) \neq 0$ in (5) leads to the non–singularity of every matrix in (14).

It can be proved that if $N$ is large enough, an estimate of the standard deviation $\sigma_\varepsilon$ of the process $\varepsilon(t)$ in (5), is given by [Ljung, 1999]

$$\sigma_\varepsilon = \sqrt{\frac{\det(\mathbf{S}_n)}{N\det(\mathbf{H}_n^T\mathbf{H}_n)}}. \tag{15}$$

If the following, the quantity $\sigma_{\varepsilon_k}$ is defined,

$$\sigma_{\varepsilon_k} = \sqrt{\frac{\det(\mathbf{S}_k)}{N\det(\mathbf{H}_k^T\mathbf{H}_k)}}. \tag{16}$$

it can be shown that $\sigma_{\varepsilon_h} > \sigma_{\varepsilon_k}$ for $h < k$, $\sigma_{\varepsilon_k} > \sigma_\varepsilon$ for $k < n$ and $\sigma_{\varepsilon_k} \cong \sigma_\varepsilon$ for $k \geq n$.

In other words, if $N$ is large enough, a sequence of decreasing values of $\sigma_{\varepsilon_k}$ followed by a stabilisation once the correct order is reached, can be noted. The criterion can be used to evaluate a suitable order or, at least, an interval of admissible orders for the model before computing its parameters.

It is easy to show that $\sigma_{\varepsilon_k}^2 = J_k(\theta)$ for an ARX model with order $k$ and parameters $\theta$ given by (11).

If the value (16) is expressed as percentage of the standard deviation of the measured output, the well-established Predicted Per Cent Reconstruction Error criterion (PPCRE) is obtained [Guidorzi and Rossi, 1974]. The PPCRE($k$) gives the prediction error of an ARX model of order $k$ without requiring any computation of its parameters and predictions. The application of the PPCRE criterion consists in computing an increasing sequence of PPCRE($k$) (or $J_k(\theta)$) and in selecting the minimal order that, once increased, does not lead to a significantly better performance.

An example of the PPCRE($k$) and $J_k(\theta)$ increasing sequences with ARX model order $k$ is reported in Figures (2(a)) and (2(b)).

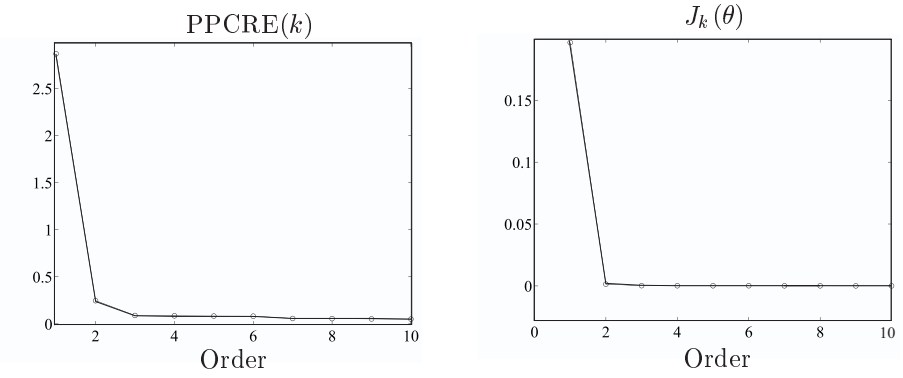


(a) (b)

Figure 2: (a) Predicted reconstruction error and (b) mean square errors for different ARM model orders $k$

Relation (16) can also be used in the application of the well-known FPE, AIC and MDL order estimation criteria [Söderström and Stoica, 1987].

# 5 Linear MISO system identification

In this section, the well-established Frisch scheme procedure for the identification of dynamic MISO system from input-output $\mathbf{u}(t) \in \Re^r$, $\mathbf{y}(t) \in \Re^m$ (with $m = 1$) noisy (fault-free) sequences will be summarised.

A finite sequence of the variables $\{u_1(t), \cdots, u_r(t), y(t)\}$ observed with a constant sampling interval is considered. If dynamic linear relations exist among these variables, they can be described by models of the type

$$y^*(t) = \sum_{i=1}^{n} \alpha_i y^*(t-i) + \sum_{k=1}^{r} \sum_{i=1}^{n} \beta_{i,k} u_k^*(t-k) \tag{17}$$

which describe linear MISO (multiple-input, single output) discrete-time systems whose order is $n$ and whose parameters are $\alpha_i$ and $\beta_{i,k}$.

At first, the following problem is presented.

**Problem 1 (realisation)** *Given a noiseless input-output sequence $\{u_1(t), \cdots, u_r(t), y(t)\}$ generated by a system of type (17), determine the order $n$ and the parameters $\alpha_i$ and $\beta_{i,k}$ of the system.*

The following vectors and matrices can be defined

$$\mathbf{u}_j^{*N}(t-k) = \left[ \begin{array}{cccc} u_j^*(t-k) & \cdots & u_j^*(t-k+N-1) \end{array} \right]^T, \tag{18}$$

$$\mathbf{y}^{*N}(t-k) = \left[ \begin{array}{cccc} y^*(t-k) & \cdots & y^*(t-k+N-1) \end{array} \right]^T, \tag{19}$$

$$\mathbf{X}_k(u_j^*) = \left[ \begin{array}{ccc} \mathbf{u}_j^{*N}(t-k) & \cdots & \mathbf{u}_j^{*N}(t-2) \end{array} \right], \tag{20}$$

$$\mathbf{X}_k(y^*) = \left[ \begin{array}{ccc} \mathbf{y}^{*N}(t-k) & \cdots & \mathbf{y}^{*N}(t-1) \end{array} \right], \tag{21}$$

$$\Sigma_k^*(u_j^* u_j^*) = \mathbf{X}_k^T(u_j^*)\mathbf{X}_k(u_j^*), \tag{22}$$

$$\Sigma_k^*(y^* y^*) = \mathbf{X}_k^T(y^*)\mathbf{X}_k(y^*), \tag{23}$$

$$\Sigma_k^*(y^* u_j^*) = \Sigma_k^*(u_j^* y^*) = \mathbf{X}_k^T(y^*)\mathbf{X}_k(u_j^*) = \mathbf{X}_k^T(u_j^*)\mathbf{X}_k(y^*), \tag{24}$$

where $N$ is assumed large enough to solve the problem considered.

The matrix $\Sigma_k^*$ is partitioned as follows

$$\Sigma_k^* = \left[ \begin{array}{cccc} \Sigma_k^*(y^*y^*) & \Sigma_k^*(y^*u_1^*) & \cdots & \Sigma_k^*(y^*u_r^*) \\ \Sigma_k^*(u_1^*y^*) & \Sigma_k^*(u_1^*u_1^*) & \cdots & \Sigma_k^*(u_1^*u_r^*) \\ \vdots & \vdots & \ddots & \vdots \\ \Sigma_k^*(u_r^*y^*) & \Sigma_k^*(u_r^*u_1^*) & \cdots & \Sigma_k^*(u_r^*u_r^*) \end{array} \right], \tag{25}$$

To solve the realisation problem it is possible to consider the sequence of increasing-dimension matrices

$$\Sigma_2^* \quad \Sigma_3^* \quad \cdots \quad \Sigma_k^* \quad \cdots \tag{26}$$

testing their singularity. As soon as a singular matrix $\Sigma_k^*$ is found then the order $n = k - 1$ and the parameters $\alpha_1, \cdots, \alpha_n, \beta_{1j}, \cdots, \beta_{nj}$ $(j = 1, \cdots, r)$ describe the dependence relationship of the $n$–th vector of $\Sigma_{n+1}^*$ on the remaining ones.

In Problem 1 it has been assumed that $N$ is large enough to avoid unwanted linear dependence relationships due to limitations in the dimension of the involved vector spaces; this means $N \geq (r+1)n + 1$. The minimal number of samples must be therefore equal to $(n+2)r + 1$. If a lower number of samples is available then only a partial realisation problem can be solved.

In the noisy case the following identification problem can be proposed.

**Problem 2 (identification)** *Given a noiseless input-output sequence* $\{u_1(t), \cdots, u_r(t), y(t)\}$ *unequivocally determine, if possible, the order* $n$ *and the parameters* $\alpha_i$ *and* $\beta_{i,k}$ *of a model (17) of the system which has generated the noiseless sequences* $\{u_1^*(t), \cdots, u_r^*(t), y^*(t)\}$.

Note that in presence of noise the procedure described for the solution of Problem 1 would obviously be useless since matrices $\Sigma_k^*$ would always be non-singular.

In the Frisch scheme it is normally assumed that

$$\begin{cases} u_j(t) &= u_j^*(t) + \tilde{u}_j(t) \qquad j = 1, \cdots, r \\ y(t) &= y^*(t) + \tilde{y}(t), \end{cases} \tag{27}$$

where every noise term $\tilde{u}_j(t)$ and $\tilde{y}(t)$ is independent of every other term $u_j(t)$ and $y(t)$ only and are known. Without loss of generality, all the variables may be assumed as having null mean value. Consequently the generic positive definite matrix $\Sigma_k$ associated with the input-output noise-corrupted sequences may always be expressed as the sum of two terms

$$\Sigma_k = \Sigma_k^* + \tilde{\Sigma}_k \tag{28}$$

where

$$\tilde{\Sigma}_k = \text{diag}\left[ \begin{array}{cccc} \tilde{\sigma}_y \mathbf{I}_k & \tilde{\sigma}_{u_1} \mathbf{I}_{k-1} & \cdots & \tilde{\sigma}_{u_r} \mathbf{I}_{k-1} \end{array} \right] \geq \mathbf{0} \tag{29}$$

since no correlation has been assumed among the noise samples at different times. This condition is verified for additive white noise with variance $\tilde{sigma}_{u_j}$ and $\tilde{sigma}_y$ on the input-output sequences.

**Problem 3** *Given a sequence of increasing-dimension* $((r+1)\,k - r) \times ((r+1)\,k - r)$ *symmetric positive definite covariance matrices*

$$\Sigma_2 \quad \Sigma_3 \quad \cdots \quad \Sigma_k \quad \cdots \tag{30}$$

*find, for each* $k$*, all diagonal non-negative definite matrices* $\tilde{\Sigma}_k = diag\left[ \begin{array}{cccc} \tilde{\sigma}_y \mathbf{I}_k & \tilde{\sigma}_{u_1} \mathbf{I}_{k-1} & \cdots & \tilde{\sigma}_{u_r} \mathbf{I}_{k-1} \end{array} \right]$ *such that*

$$\Sigma_k^* = \Sigma_k - diag\left[ \begin{array}{cccc} \tilde{\sigma}_y \mathbf{I}_k & \tilde{\sigma}_{u_1} \mathbf{I}_{k-1} & \cdots & \tilde{\sigma}_{u_r} \mathbf{I}_{k-1} \end{array} \right] \geq \mathbf{0}. \tag{31}$$

It is worth observing now that, unlike the algebraic case, for each $k$ the noise space is always $\Re_+^{(r+1)}$, while the parameter space is $\Re^{((r+1)k-r)}$.

We can note that for each $k$ the solution set of the previous relation describes, in the first orthant of the $(\sigma_y, \sigma_{u_1}, \cdots, \sigma_{u_r})$ hyper-plane, a hyper-surface whose concavity faces the origin [Beghelli et al., 1990].

Previous results hold for every value of $k$. Since determination of the system order requires the increasing values of to be tested, it is relevant to analyse the behaviour of the associated curves when varies. This corresponds to a comparison of the admissible solution sets for different model orders. In this context the following result can be proved [Beghelli et al., 1990].

**Theorem 1** *The solution sets of condition* $\Sigma_k^* \geq \mathbf{0}$ *for different values of* $k$ *are non-crossing curves [Beghelli et al., 1990].*

It is also important to observe that, since we assume that a system (17) has generated the noiseless data, for $k > n$ all the hyper–surfaces of type $\Sigma_k^* \geq \mathbf{0}$ have necessarily at least one common point, i.e. the point $\left(\sigma_y^*, \sigma_{u_1}^*, \cdots, \sigma_{u_r}^*\right)$ corresponding to the true variances $\sigma_{u_j}^*$ and $\sigma_y^*$ of the noise affecting the inputs and the output of the system, respectively. The search for a solution for the identification problem can thus start from the determination in the noise space of this point.

The following considerations can now be stated.

With reference to the diagonal non–negative definite matrices

$$\tilde{\Sigma}_k = \text{diag}\left[ \begin{array}{cccc} \tilde{\sigma}_y \mathbf{I}_k & \tilde{\sigma}_{u_1} \mathbf{I}_{k-1} & \cdots & \tilde{\sigma}_{u_r} \mathbf{I}_{k-1} \end{array} \right] \geq \mathbf{0} \tag{32}$$

the following properties hold:

- If $k \leq n$ the matrices $\Sigma_k^*$ are positive definite.
- If $k > n$ the dimension of the null space of $\Sigma_k^*$ and, consequently, the multiplicity of its least eigenvalue, is equal to $k - n$.
- For $k = n + 1$, the matrix $\Sigma_k^*$ is characterised by a linear dependence relation among its $((r+1)k - r)$ vectors and the coefficients which link the $k$–th vector of $\Sigma_k^*$ to the remaining ones are the parameters $\alpha_i$ and $\beta_{ij}$, with $i = 1, \cdots, n$ and $j = 1, \cdots, r$, of the system (17) which has generated the noiseless sequences.
- For $k > n + 1$ all linear dependence relations among the vectors of the matrix $\Sigma_k^*$ are characterised by the same coefficients $\alpha_i$ and $\beta_{ij}$.

If $m$ models of the type (17) are used to describe the mathematical behaviour of a multivariable dynamic system with $r$ inputs and $m$ outputs $\mathbf{y}(t)$, the previous identification procedure must be repeated $m$ times. At every step the identification procedure must lead to the same values for the input noise variances $\left(\sigma_y^*, \sigma_{u_1}^*, \cdots, \sigma_{u_r}^*\right)$.

It is worthy to note how this approach cannot be applied immediately in the identification of real processes, since the hypotheses on the linearity, finite dimensionality and time independence of the system and on the additivity and whiteness of the noise are not usually verified, so that the hyper–surfaces $\Sigma_k^* \geq \mathbf{0}$ have no common point for $k > n$. The definition of a suitable criterion of model selection in such cases was suggested in [Beghelli et al., 1994].

As an example, Figure (3) shows the above properties for a SISO ($m = r = 1$) dynamic system with $n = 2$. The point marked with a circle corresponds to the input-output noise variances $\sigma_y^*$ and $\sigma_u^*$ affecting the measurements.

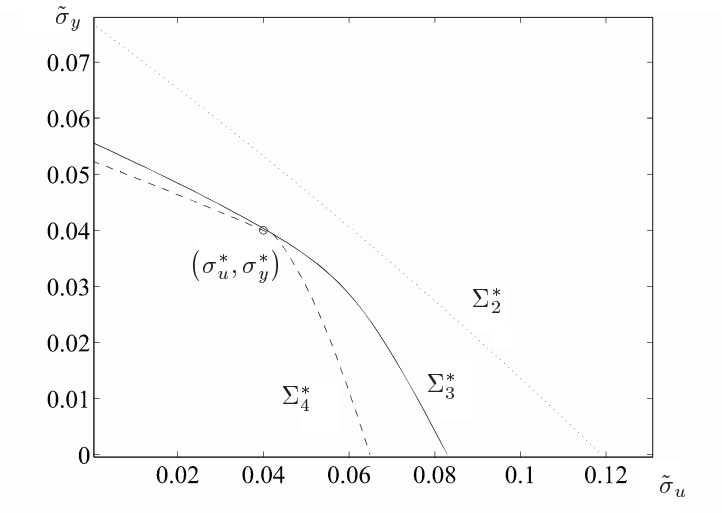


Figure 3: Singularity surfaces in the noisy space for $n = 2$

# 6 Residual generation

The problem treated in this work regards the detection and isolation of the faults on the basis of the knowledge of the measured sequences $\mathbf{u}(t)$ and $\mathbf{y}(t)$. The structure of the fault detection device is depicted in Figure (4).

The symptom (residual, $\mathbf{r}(t)$) generation is implemented by means of dynamic observers or Kalman filters, driven by $\mathbf{u}(t)$ and $\mathbf{y}(t)$, in order to produce a set of signals, $\mathbf{f}(t)$, from which it

will be possible to isolate faults associated to actuators, components and sensors. The symptom evaluation refers to a logic device which processes the redundant signals generated by the first block in order to estimate and unequivocally identify a fault occurrence.

This report will present a FDI technique to elaborate a set of symptoms from which it will be possible to unequivocally detect faults. With reference to Figure (4) the symptom signals are differences between estimated signals (given by observers or Kalman filters) and the actual ones supplied by the input and output sensors.

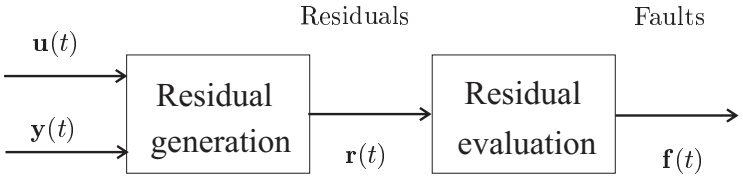


Figure 4: Logic diagram of the fault detection system.

Moreover, it is assumed that only a single fault may be present in the actuators, components or input sensors of the plant at any given time. On the other hand, multiple output sensor faults can be handled.

# 7 Fault diagnosis in a deterministic environment

The aim of this report consists in finding a procedure in order to detect and isolate faults on actuators, components and sensors of single-shaft industrial gas turbine. The model of such a turbine was developed in SIMULINK© environment [MathWorks, 1992].

Figure (5) shows the gas turbine layout as well as its inputs and outputs.

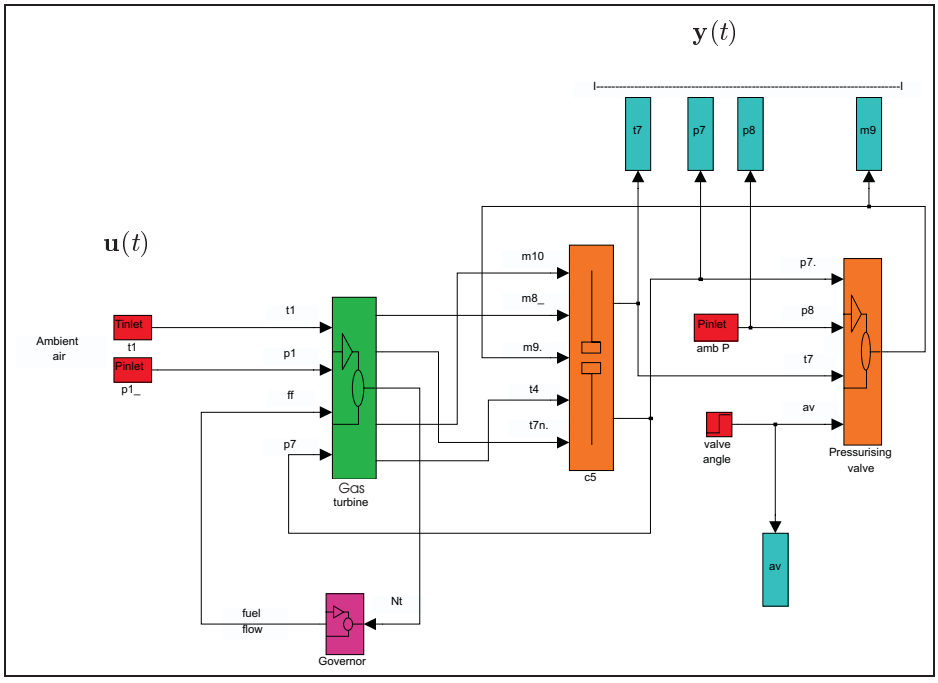


Figure 5: The monitored system.

The time series of data used to identify the models were generated with a non–linear dynamic model in SIMULINK© environment and they simulate measurements taken on the machine with a sampling

rate of 0.08s and without noise ($\tilde{\mathbf{u}}(t) = \mathbf{0}$ and $\tilde{\mathbf{y}}(t) = \mathbf{0}$) due to measurement uncertainty which, instead, is always present in the real measurement systems.

The non–linear SIMULINK© model of the gas turbine was validated in steady state conditions against engine measurements where available, and against the prediction of a more rigorous steady state gas turbine model where measurements were not available. The SIMULINK© model variables were found to be within 5% of the measured and rigorous modeled values. For the majority of variables the accuracy was within 1%.

In the dynamic case no model validation has been carried out as yet.

Orders and output reconstruction errors of each ARX model are shown in Table (2). The $i$–th model (with $i = 1, \cdots, m$ and $m = 28$) is driven by $a_v(t)$ and $f_f(t)$ and gives the prediction of the $i$–th output $y_i(t)$.

The inputs are $\mathbf{u}(t) = [a_v(t), f_f(t)]$ and they are summarised in Table (1). Table (1) also reports measurement accuracy, nature (e.g. measured or inferred) and reference values.

| Variable | Name | Nature | Accuracy | Ref |
|---|---|---|---|---|
| $t_1$ | amb. air temp. | measured | $\pm 0.4^o C$ | 273.6 |
| $p_1$ | amb. air press. | inferred | | 100900 |
| $f_f$ | fuel flow | inferred | $\pm 5\%$ | 0.21654 |
| $a_v$ | valve angle | measured | $\pm 2\%$ | 63.15 |

Table 1: Dynamic model identification: turbine inputs

The input signals $a_v(t)$ and $f_f(t)$ are shown in Figures (6(a)) and (6(b)).

Even if, according to Figure (5) the measurements of ambient and pressure temperature ($p_1$ and $t_1$) are inputs for the turbine, they were not considered, since they are constant all the times.

The outputs are $y(t) = [\ m_1,\ m_3,\ m_4,\ m_5,\ m_6,\ m_8,\ m_9,\ p_2,\ p_3,\ p_4,\ p_5,\ p_7,\ p_t,\ q_a,\ q_c,\ q_t,\ t_3,\ t_{3n},\ t_4,\ t_{4n},\ t_5,\ t_{5n},\ t_6,\ t_7,\ w_t]$ and they are collected in Table (2). Table (2) also shows measurement accuracy, nature (e.g. measured or inferred) and reference values.

Each model was tested in different operating conditions and it has always provided an output reconstruction error lower than 0.5%.

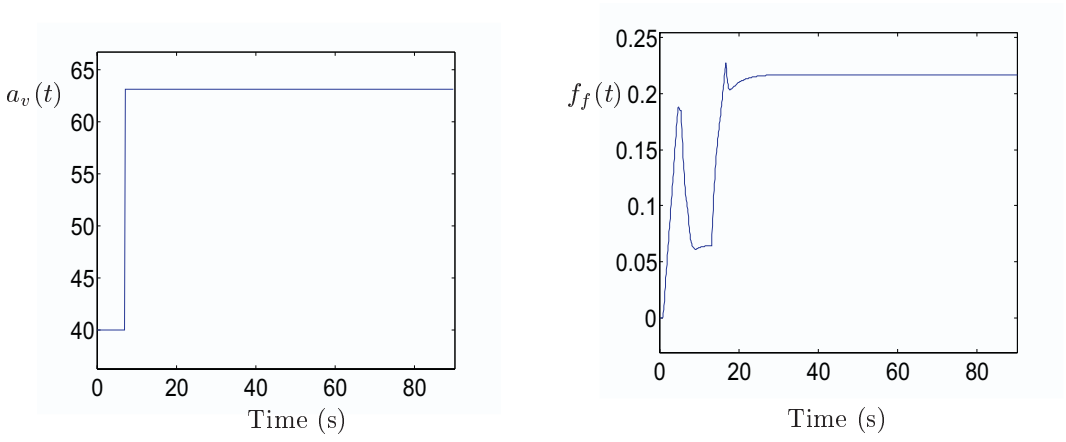


(a) $u_1(t) = a_v(t)$ (b) $u_2(t) = f_f(t)$

Figure 6: Gas turbine input signals: (a) valve angle and (b) fuel flow.

Moreover, two time series of data generated by the gas turbine non–linear model were exploited in order to validate the ARX models.

These models have always provided in full simulation an output reconstruction error lower than 1%.

| Variable | Name | Model order | SSE | Nature | Accuracy | Ref |
|---|---|---|---|---|---|---|
| $m_1$ | mass flow | 4 | 0.00079 | inferred | $\pm 5\%$ | 16.8162 |
| $m_3$ | | 2 | $2.83 \times 10^{-5}$ | inferred | $\pm 5\%$ | 16.8163 |
| $m_4$ | | 2 | $4.13 \times 10^{-5}$ | inferred | $\pm 5\%$ | 16.8332 |
| $m_5$ | | 2 | $3.39 \times 10^{-5}$ | inferred | $\pm 5\%$ | 13.3269 |
| $m_6$ | | 2 | $2.19 \times 10^{-5}$ | inferred | $\pm 5\%$ | 1.9946 |
| $m_8$ | turb. outlet mass flow | 2 | $2.12 \times 10^{-5}$ | inferred | $\pm 5\%$ | 15.5561 |
| $m_9$ | press. valve mass flow | 3 | 0.0060 | inferred | $\pm 5\%$ | 17.0321 |
| $p_2$ | comp. inlet temp. | 2 | 0.00035 | measured | $\pm 1\%$ | 100005.1466 |
| $p_3$ | comp. exit press. | 2 | $2.00 \times 10^{-5}$ | measured | $\pm 2\%$ | 1026228.281 |
| $p_4$ | | 2 | $2.10 \times 10^{-5}$ | measured | | 989222.4985 |
| $p_5$ | | 2 | $2.30 \times 10^{-5}$ | measured | | 939569.728 |
| $p_7$ | turb. back press. | 2 | 0.00018 | measured | | 202094.0779 |
| $p_t$ | power | 2 | $2.98 \times 10^{-5}$ | inferred | | 5312941.3134 |
| $q_a$ | torque | 2 | 0.00062 | inferred | $\pm 5\%$ | 1.5424 |
| $q_c$ | torque | 2 | $6.03 \times 10^{-5}$ | inferred | $\pm 5\%$ | 3142.3523 |
| $q_t$ | torque | 2 | $4.64 \times 10^{-5}$ | inferred | $\pm 5\%$ | 3199.5385 |
| $t_3$ | comp. exit temp. | 2 | $4.84 \times 10^{-5}$ | measured | $\pm 1.5^oC$ | 578.5786 |
| $t_{3n}$ | | 2 | $1.13 \times 10^{-5}$ | inferred | | 578.5759 |
| $t_4$ | turbine cooling air temperature | 2 | $5.18 \times 10^{-5}$ | inferred | | 578.5657 |
| $t_{4n}$ | | 2 | $4.84 \times 10^{-5}$ | inferred | | 578.5786 |
| $t_5$ | comb. exit temp. | 2 | 0.00036 | measured | $\pm 1.5^oC$ | 1225.0295 |
| $t_{5n}$ | | 2 | $5.18 \times 10^{-5}$ | inferred | | 578.5657 |
| $t_6$ | | 2 | 0.00036 | inferred | | 1148.1068 |
| $t_7$ | pressure valve up stream temperature | 2 | 0.00042 | measured | $\pm 1.5^oC$ | 839.6036 |
| $w_t$ | turb. speed | 2 | $5.31 \times 10^{-5}$ | measured | $\pm 1\%$ | 1660.8553 |

Table 2: Turbine outputs and MISO ARX model characteristics.

A very effective way of evaluating the adequacy and flexibility of identified models consists, in fact, in their use for performing complete simulations (i.e. using only the initial samples of the observed outputs) and in comparing the obtained predictions with observed output samples. This procedure, that can be applied when a single set of data is available, gives the best results when applied to sequences different from those used to identify the model. The mean square prediction error between the observed outputs and the ones obtained by simulation can be used to compare models with different orders.

Reconstruction errors of each ARX model are summarised in Table (3).
In the following, the deterministic FDI problem is solved via the implementation of a bank of output observers.

# 8 Simulated Fault Conditions

Four gradually developing faults are represented as follows:

1) Compressor contamination (core engine performance deterioration), $f_s(t)$.

2) Thermocouple sensor fault (output sensor failure), $f_y(t)$.

| Variable | Model order | SSE | 1st valid. | 2nd valid. | Ref |
|---|---|---|---|---|---|
| $m_1$ | 4 | 0.00079 | 0.00264 | 0.78999 | 16.8162 |
| $m_3$ | 2 | $2.83 \times 10^{-5}$ | 0.00011 | 0.0791 | 16.8163 |
| $m_4$ | 2 | $4.13 \times 10^{-5}$ | 0.00017 | 0.0792 | 16.8332 |
| $m_5$ | 2 | $3.39 \times 10^{-5}$ | 0.00013 | 0.00552 | 13.3269 |
| $m_6$ | 2 | $2.19 \times 10^{-5}$ | $4.84 \times 10^{-5}$ | 0.0040 | 1.9946 |
| $m_8$ | 2 | $2.12 \times 10^{-5}$ | $9.12 \times 10^{-5}$ | 0.0078 | 15.5561 |
| $m_9$ | 3 | 0.0060 | 0.00049 | 0.0058 | 17.0321 |
| $p_2$ | 2 | 0.00035 | 0.0023 | 0.12255 | 100005.1466 |
| $p_3$ | 2 | $2.00 \times 10^{-5}$ | $5.05 \times 10^{-5}$ | 0.8177 | 1025666.281 |
| $p_4$ | 2 | $2.10 \times 10^{-5}$ | $5.10 \times 10^{-5}$ | 0.7704 | 989222.4985 |
| $p_5$ | 2 | $2.30 \times 10^{-5}$ | $5.14 \times 10^{-5}$ | 0.8255 | 939569.728 |
| $p_7$ | 2 | 0.00018 | 0.00011 | 0.0795 | 202094.0779 |
| $p_t$ | 2 | $2.98 \times 10^{-5}$ | $7.28 \times 10^{-5}$ | 0.0841 | 5312941.3134 |
| $q_a$ | 2 | 0.00062 | 0.00029 | 0.9736 | 1.5424 |
| $q_c$ | 2 | $6.03 \times 10^{-5}$ | $8.49 \times 10^{-5}$ | 0.8347 | 3142.3523 |
| $q_t$ | 2 | $4.64 \times 10^{-5}$ | $4.55 \times 10^{-5}$ | 0.8745 | 3199.5385 |
| $t_3$ | 2 | $4.84 \times 10^{-5}$ | $5.53 \times 10^{-5}$ | 0.00274 | 578.5786 |
| $t_{3n}$ | 2 | $1.13 \times 10^{-5}$ | $1.02 \times 10^{-5}$ | 0.00021 | 578.5759 |
| $t_4$ | 2 | $5.18 \times 10^{-5}$ | $5.98 \times 10^{-5}$ | 0.02083 | 578.5657 |
| $t_{4n}$ | 2 | $4.84 \times 10^{-5}$ | $5.53 \times 10^{-5}$ | 0.00274 | 578.5786 |
| $t_5$ | 2 | 0.00036 | 0.00012 | 0.1042 | 1225.0295 |
| $t_{5n}$ | 2 | $5.18 \times 10^{-5}$ | $5.98 \times 10^{-5}$ | 0.02083 | 578.5657 |
| $t_6$ | 2 | 0.00036 | 0.00012 | 0.1042 | 1148.1068 |
| $t_7$ | 2 | 0.00042 | 0.00012 | 0.04270 | 839.6036 |
| $w_t$ | 2 | $5.31 \times 10^{-5}$ | $5.99 \times 10^{-5}$ | 0.31424 | 1660.8553 |

Table 3: Dynamic ARX model validation

3) High Pressure turbine seal damage (core engine performance deterioration), $f_s(t)$ .

4) Fuel actuator friction wear (controller fault), $f_c(t)$.

Note that in real industrial applications it is commonplace for each of the above faults to develop slowly over a period of months. For the purpose of this simulation - in order to avoid excessively long duration simulations - the fault development rate will be increased so that significant effects are present after one hour. However this is still considerably longer than the duration of the gas turbine dynamics which occur over periods of seconds - a factor which must be taken account of in any FDI algorithm design.

With reference to the block scheme of the monitored system depicted in Figure (1), the fault generation model with respect to the input and output measurements $\mathbf{u}(t)$ and $y_i(t)$ can be represented by the structure shown in Figure (7).

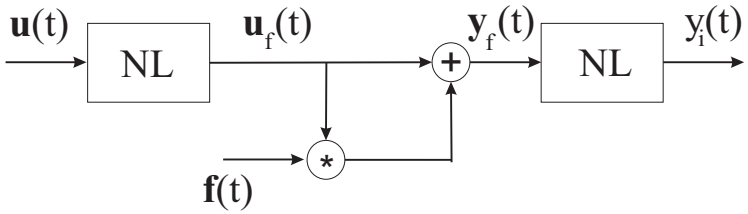


Figure 7: Fault generation logic scheme.

where NL blocks represent any non–linear dynamic relations between the input signals $\mathbf{u}(t)$ and $\mathbf{u}_f(t)$ as well as the output signals $\mathbf{y}_f(t)$ and $y_i(t)$ $(i = 1, \cdots, m)$, whilst the vector $\mathbf{f}(t)$ may represent the faults $\mathbf{f}_s(t)$, $\mathbf{f}_y(t)$ or $\mathbf{f}_c(t)$. The non–linear relation among $\mathbf{u}_f(t)$, $\mathbf{y}_f(t)$ and $\mathbf{f}(t)$ is performed by the the inner block, shown in Figure (7), multiplying $\mathbf{f}(t)$ by $\mathbf{u}_f(t)$ and adding them to $\mathbf{u}_f(t)$ itself in order to obtain $\mathbf{y}_f(t)$.

$$\mathbf{y}_f(t) = \mathbf{u}_f(t) + \mathbf{u}_f(t) * \mathbf{f}(t). \tag{33}$$

In particular, with reference to the system under investigation, Figure (7) represents the non–linear link between the faults $\mathbf{f}(t)$ and the input-output signals $\mathbf{u}(t)$, $y_i(t)$.

In the presence of a fault condition, the challenge for the designer of an FDI algorithm may be summarised as follows:

1. Detect that a fault condition exists with minimum delay from the initial occurrence of the fault.

2. Identify the nature, magnitude and location of the fault, again with minimum delay from the initial occurrence of the fault.

Note that it is desirable to avoid introducing perturbation signals onto the model variables. In the first instance an FDI design should be based upon data which is available from the normal day to day operation of the plant, for example during transient and over prolonged periods of steady state operations.

The rate of development and magnitude of faults have been set to nominal values in this case study. It will be of interest to know how small the fault parameters can be made whilst still maintaining good FDI performance.

## 8.1 Case 1: compressor contamination (*core engine* performance deterioration)

Failure "case 1", represents fouling of the surfaces of the compressor blades, this reduces air flow, changes the blade aerodynamics and consequently changes the surface roughness. The failure is modeled as a gradual decrease in mass flow rate for a given pressure ratio. With reference to Figure (7) (with $\mathbf{u}_f(t) = in\_1$ and $\mathbf{y}_f(t) = out\_1$), the fault $f_s(t)$ affects the monitored system of Figure (1) by means of the SIMULINK© submodel shown in Figure (8).

The maximum decrease in mass flow rate is set nominally at 5% while the fault development rate is set to (5% decrease of normal flow rate)/hour.

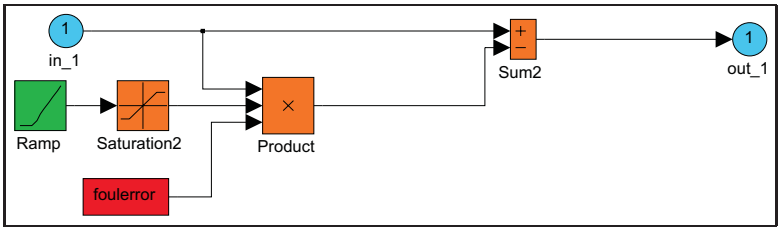


Figure 8: Fault "case 1" SIMULINK submodel.

In order to design the component $(f_s(t) \in \Re)$ FDI scheme ($\mathbf{f}_u(t) = \mathbf{0}$, $\mathbf{f}_y(t) = \mathbf{0}$ and $\mathbf{f}_c(t) = \mathbf{0}$), with respect to the turbine SIMULINK© model, the subsystem depicted in Figure (9) was considered. The inputs for the subsystem are $p_2$, $p_3$, $\omega_t$ and $t_2$, while $m_3$, $q_c$ and $t_3$ are the outputs directly affected by the fault $f_s(t)$.

The most sensitive output signal to a ramp fault is $q_c(t)$, which is depicted in Figure (10(a)). In Figure (10(b)) the ramp fault $f_s(t)$ is shown.

It is worthy to note how the shape of $q_c(t)$ transient is determined by the input variation, depicted in Figures (6(a)) and (6(b)), not by the slowly developing compressor hauling fault $f_s(t)$ (which is also of very small magnitude). $q_c(t)$ signal and $f_s(t)$ fault have, in fact, very different magnitudes.

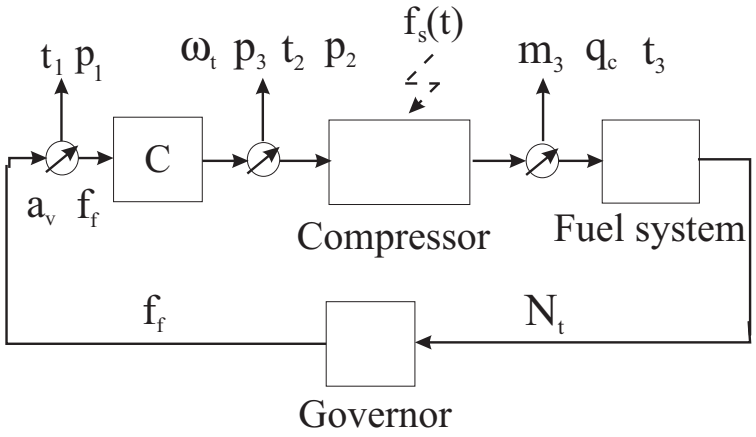


Figure 9: The monitored subsystem

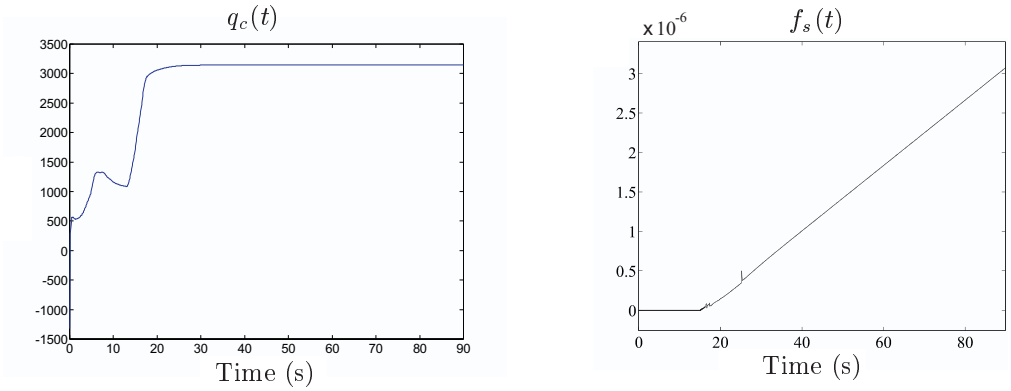


(a) $q_c(t)$ output

(b) $f_s(t)$ fault

Figure 10: (a) The monitored signal $q_c(t)$ and (b) the component fault mode $f_s(t)$.

A second order ($n = 2$) ARX MISO ($r = 2$, $m = 1$) model was identified with an output reconstruction error $J(\theta) = 6.03 \times 10^{-5}$. The parameters of such a model, driven by $a_v(t)$ and $f_f(t)$ signals, are represented by the vector $\theta = [-0.9246, 1.9238, -0.0009, 0.0010, -0.0353, 0.0359]$. The diagnosis of the $q_c(t)$ signal (linked to the faulty turbine component) requires the knowledge of the triple ($\mathbf{A}_i$, $\mathbf{B}_i$, $\mathbf{C}_i$) with $i = 13$ and the identification of an ARX model with two inputs which gives the prediction of the 13–th output $q_c(t)$. Because of the deterministic case, in which $\tilde{\mathbf{u}}(t) = \mathbf{0}$, $\tilde{\mathbf{y}}(t) = \mathbf{0}$ in the system (6) the term $\varepsilon_i(t)$ was neglected ($\varepsilon_i(t) = 0$).

The detection of a fault regarding the compressor was performed by using the classical output observer configuration exploited for the FDI of output sensor faults, as depicted in Figure (11(a)). The inputs $a_v(t)$, $f_f(t)$ and the output $q_c(t)$ feed the observer to estimate the signal $q_c(t)$ itself and to generate the residual $r(t)$. The poles $\mathbf{p}$ of the output observer for the signal $q_c(t)$ were chosen near 0.5 according to the minimisation of the function $V(\mathbf{p})$, shown in Figure (11(b)).
The eigenvalues $\mathbf{p} = [\ p_1 \quad \cdots \quad p_n\ ]$, in fact, were chosen to maximise the mean square error of the residual sensitivity $r(t, \mathbf{p})|_f$ to a fault and minimise the mean square error of the residual in fault-free

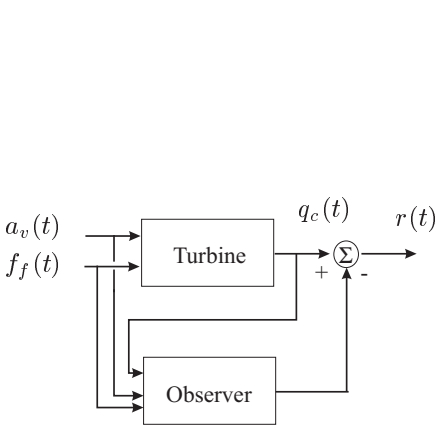


(a) $q_c(t)$ residual generator

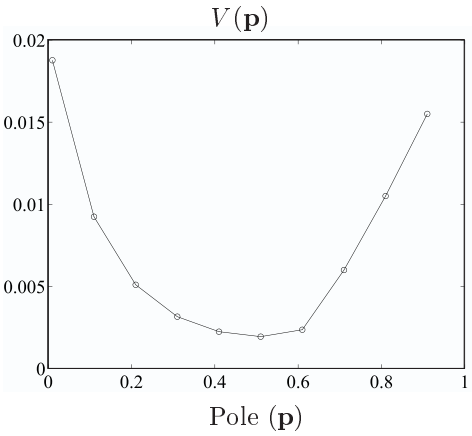


(b) Pole assignment cost function

Figure 11: (a) observer scheme and (b) $V(\theta)$ cost function.

condition, $r(t,\mathbf{p})|_h$. The minimum $\min_p V(\mathbf{p})$, where $V(\mathbf{p})$ is the cost function

$$V(\mathbf{p}) = \frac{||r(t,\mathbf{p})||_h^2}{||r(t,\mathbf{p})||_f^2} \tag{34}$$

has to be found.

In Figure (11(b)), the plot of $V(\mathbf{p})$ with $\mathbf{p} = p_n$ and $p_1 = p_2 = \cdots = p_{n-1} = 0.5$ is shown.

Figure (12(a)) shows the estimate of the fault $f_s(t)$ obtained by computing the difference between the fault–free (solid line) and the faulty residual (dotted line), depicted in Figure (12(b)).

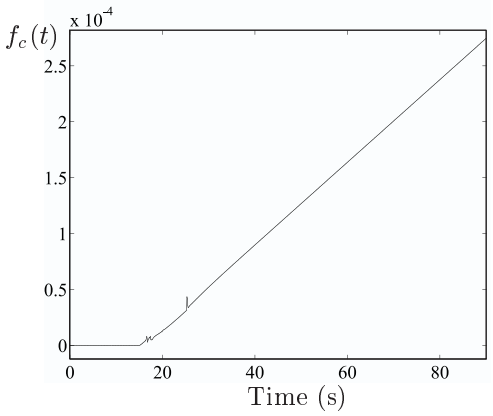


(a) $f_c(t)$ fault estimate

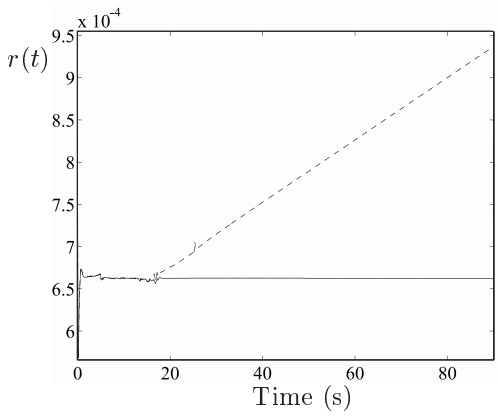


(b) Fault-free and faulty residual $r(t)$

Figure 12: (a) the fault model and (b) the fault-free and faulty residual.

## 8.2 Case 2: fault diagnosis of the output sensor.

Failure "case 2" represents the malfunctioning of a thermocouple in the gas path leading to a slowly increasing or decreasing reading over time. With reference to Figure (7) (with $\mathbf{u}_f(t) = in\_1$ and

$\mathbf{y}_f(t) = out\_1$), the fault on the measurement of the $t_{3n}$ output variable affects the output sensor by means of the SIMULINK© model depicted in Figure (13).

There is no limit placed on the error magnitude while the fault development rate is set to (5% error in measuring actual temperature)/hour.

In order to diagnose a single $f_{y_i}(t)$ fault on the $i$–th output sensor ($\mathbf{f}_u(t) = \mathbf{0}$, $\mathbf{f}_s(t) = \mathbf{0}$, $\mathbf{f}_c(t) = \mathbf{0}$ and $\varepsilon_i(t) = 0$) when the measurement noises are negligible ($\tilde{\mathbf{u}}(t) = \mathbf{0}$ and, $\tilde{\mathbf{u}}(t) = \mathbf{0}$), with reference to system (6), the model of the $i$–th output observer ($i = 1, \cdots, m$) has the form

$$\mathbf{x}^i(t+1) = \mathbf{A}_i\mathbf{x}^i(t) + \mathbf{B}_i\mathbf{u}^*(t) + \mathbf{K}_i\left(y_i^*(t) + f_{y_i}(t) - \mathbf{C}_i\mathbf{x}^i(t)\right) \tag{35}$$

where $\mathbf{x}^i(t)$ is the $i$–th observer state vector, $f_{y_i}(t)$ represents a fault on the $i$–th output sensor and the triple ($\mathbf{A}_i$,$\mathbf{B}_i$,$\mathbf{C}_i$) is a minimal state-space representation (completely observable) of the link among the inputs of the process and its $i$–th output $y_i^*(t)$.

In the absence of faults, it can be verified that, for the $i$–th output, the residual $r_i(t) = y_i^*(t) - y^i(t) = \mathbf{C}_i\left(\mathbf{x}_i(t) - \mathbf{x}^i(t)\right)$ is equal to zero. In the presence of a fault on the $i$–th output sensor the $i$–th output residual reaches a value different from zero and this situation leads to a complete failure diagnosis.

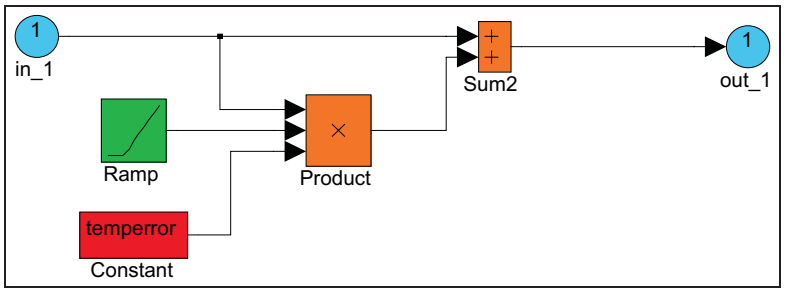


Figure 13: SIMULINK fault model of the output sensor.

In particular, the diagnosis of the $t_{3n}$ output sensor (thermocouple fault), represented in Figure (13), requires the knowledge of the triple ($\mathbf{A}_i$,$\mathbf{B}_i$,$\mathbf{C}_i$) with $i = 18$ and therefore the identification of an ARX model with two inputs which gives the prediction of the 18–th output $t_{3n}$.

A second order ARX MISO model ($r = 2$ and $m = 1$), driven by $a_v(t)$ and $f_f(t)$ input signals, was identified. Such a model gives an output reconstruction error equal to $1.13 \times 10^{-5}$. The parameters of the ARX model are described by the vector $\theta = [-0.0244,\ 1.0295,\ -0.0020,\ -0.0014,\ -0.3180,\ 0.3140]$.

The poles of the output observer, whose scheme is depicted in Figure (14(a)), were chosen near 0.3 in order to minimise the function $V(\mathbf{p})$.

As shown in Figure (14(b)), an incipient fault (drift) was generated in the output sensor of the SIMULINK© model by adding a ramp function with a slope of $0.008^o\frac{C}{s}$ to the $t_{3n}$ output signals. Moreover, it was decided to consider a fault during a transient since, in this case, the residual error due to ARX model approximation is maximum and therefore it represents the most critical case.

The fault occurring on the single sensor causes alteration of the sensor signal and of the residuals given by the output observer using this signal as input. These residuals indicate a fault occurrence when their values are lower or higher than the thresholds fixed in fault-free conditions
Figure (15(a)) shows the fault-free $y_i^*(t) - y^i(t)$ (continuous line) and faulty $y_i(t) - y^i(t)$ (dotted line) residual obtained from the difference between the values computed by the observer related to the output $y_{18}(t) = t_3n$ and the ones given by the sensor. Obviously, the non zero value of the residual is due to the ARX model approximation.

The drift (ramp fault) in Figure (15(b)) starts at the instant $t = 15$s. Since the observer gives the estimate $y^i(t)$ of $y_i(t)$ at the instant $t$ by using measurements available from the instant $t = 0$ to $t = n-1$, a fault occurring at the instant $t$ affects only $y_i(t)$. This change produces the instantaneous peak which appears in Figure (15(b)) [Simani et al., 2000a]. In such a case, the peaks are not due

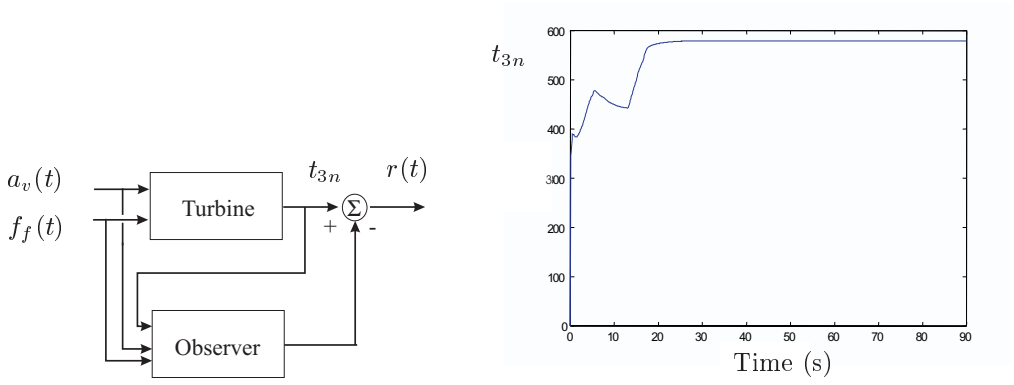


(a) Output sensor observer scheme

(b) $t_{3n}$ output measurement

Figure 14: (a) output sensor FDI configuration and (b) the output sensor signal.

to instantaneous changes in the input signals, e.g. fuel flow $f_f(t)$ or butterfly valve position $a_v(t)$. Thus, they may be used as incipient detector of anomalous behaviour of the output sensors.

Figure (15(b)) shows the behaviour of the residual with the same fault as the previous case occurring at the instant $t = 35$s in different operating conditions of the plant. The fault free residual, $y_i^*(t) - y^i(t)$, is depicted in continuous line, whilst the faulty one, $y_i(t) - y^i(t)$, using dotted line. The step which appear in the Figure (15(b)) is generated by the change related to the fault occurrence at the same instant.

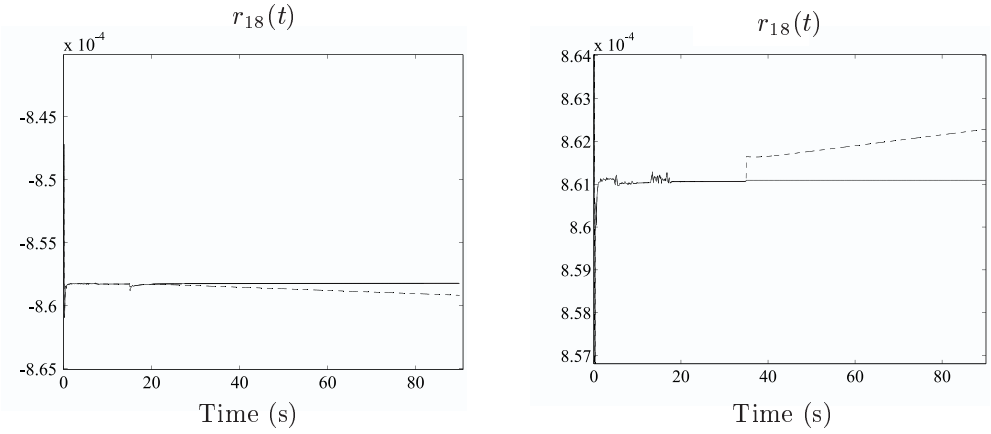


(a)

(b)

Figure 15: Residual function in different operating points.

Figure (16(a)) depicts the dynamics of the drift $f_{y_{18}}(t)$ affecting the $t_{3n}$ output sensor, while, Figure (16(b)) shows the fault estimate obtained from the difference between the fault-free and the faulty residual. The peak which appears in the Figure (16(b)) is generated by the instantaneous difference between measured $y_i(t)$ and estimated output $y^i(t)$ at the instant $t$ related to the fault occurrence. It is worthy to note how, because of the non–linear links between fault and symptom signals, the failure estimates may have different scales from the real ones. The estimate of faults can, in fact, only captures the ramp nature of the real failures but not the magnitude.

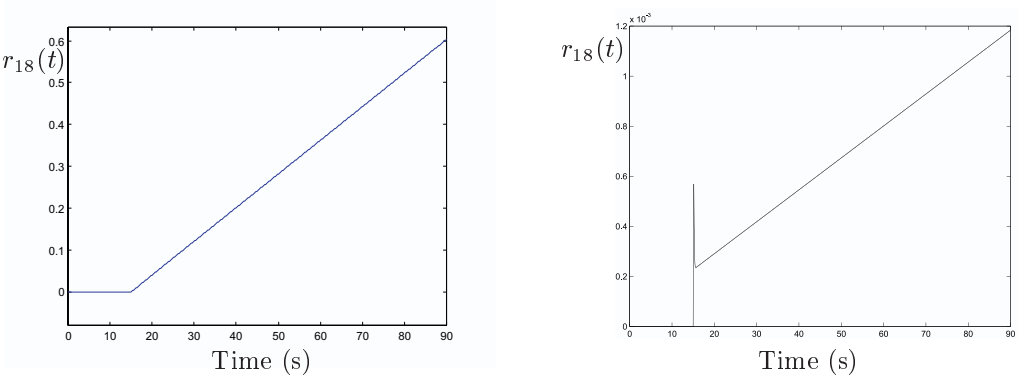


(a) Measured fault function

(b) Estimated fault signal

Figure 16: (a) real and (b) estimated fault function.

## 8.3 Case 3: high pressure seal damage (*core engine* performance deterioration)

Failure"case" represents failure $f_s(t)$ of an HP turbine seal. This results in a reduction in turbine efficiency. The fault is modeled as a gradual reduction in turbine efficiency over time. The maximum decrease in turbine efficiency is set nominally at 5% while the fault development rate is set to (5% reduction of normal efficiency)/hour.

In order to detect such a fault, an output observer fed by the inputs $a_v(t)$, $f_f(t)$ and $p_5(t)$ is designed. With reference to Figure (7), the SIMULINK© subsystem used to inject the component fault $f_s(t)$ into the monitored systems is depicted in Figure (17).

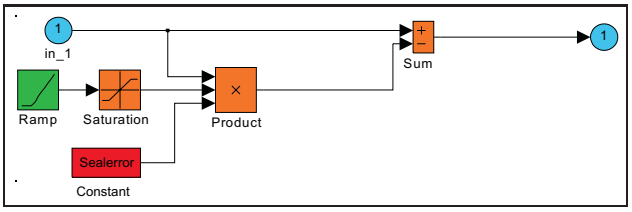


Figure 17: Fault SIMULINK subsystem

In Figure (18) the plot of the output measurement $p_5(t)$ is shown.
The component fault dynamics $f_s(t) \in \Re$ and its estimate $\hat{f}_s(t)$ obtained by the output observer are shown in Figures (19(a)) and (19(b)), respectively.
Under noise-free conditions ($\tilde{\mathbf{u}}(t) = \mathbf{0}$, $\tilde{\mathbf{y}}(t) = \mathbf{0}$), with reference to system (6) with $\varepsilon_i(t) = 0$, the observer was designed for a third order MISO model which gives a mean square reconstruction error equal to $1.8013 \times 10^{-6}$ and the eigenvalues were chosen near 0.3 to minimise the cost function $V(\mathbf{p})$. The ARX parameter vector estimated is described by $\theta = [0.4234, -1.7905, 2.3658, 0.0002, 0.0008, 0.0933, -0.2035, 0.1113]$.

The scheme used to generate the redundant residual regarding the $p_5(t)$ output signal is depicted in Figure 20(a). The fault free and the faulty residual are also shown in the Figure 20(b).

## 8.4 Case 4: Fuel *actuator* friction wear

Failure "case 4", $f_c(t)$ represents the loss of performance due to wear of the fuel valve actuator. With reference to Figure (7), the SIMULINK© model used to generate the fault signal $f_c(t) \in \Re$ is

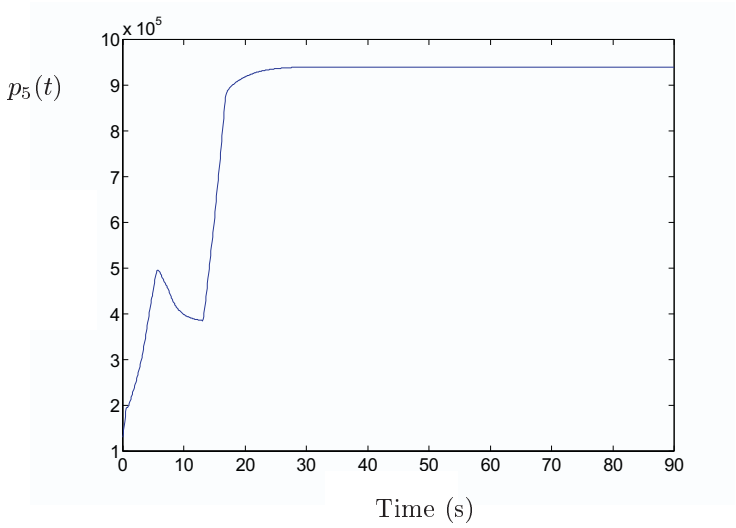


Figure 18: The $p_5(t)$ measured signal.

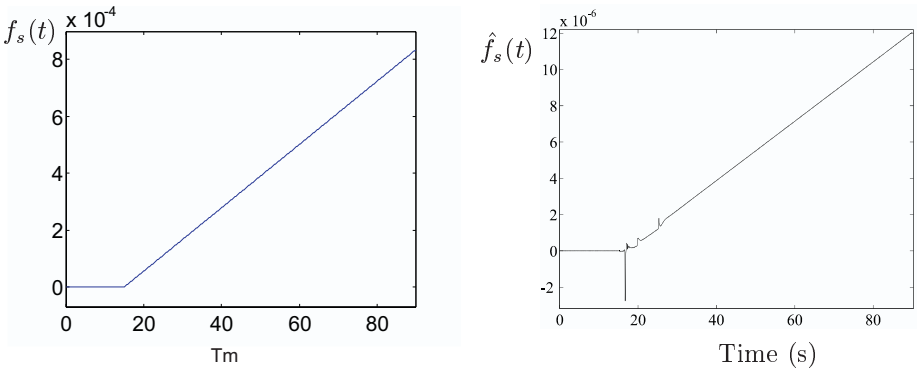


(a) Actual (b) Estimated

Figure 19: "Case 3" seal fault $f_s(t)$ dynamics

depicted in Figure (21).

As there are no specific actuator dynamics in the current model, the wear effect of the valve actuator causing slower response to demanded flow rates is modeled as a simple first order lag on the resulting fuel flow. The time constant increases linearly with the time to represent progressive wear damage to the actuator.

In order to generate the residual for the diagnosis of the actuator fault $f_c(t)$, the output observer scheme represented in Figure (22(a)) was exploited.

In particular, the inputs of the turbine, the fuel flow, $f_f(t)$, the valve angle, $a_v(t)$ and the outputs $t_6(t)$,$t_4(t)$, $p_3(t)$, $p_5(t)$ and $m_{10}(t)$ were considered. The speed demand, $\omega_d(t)$, one of the inputs of the governor and $\omega_t(t)$, the third output of the turbine were also shown.

For each output, a third order ($n = 3$) ARX model with two inputs and one output ($m = 1$, $r = 2$) was identified. By means of the SIMULINK© system (5), a single fault $f_c(t)$ was simulated and the most sensitive output to a fault regarding the actuator was determined. The $p_3(t)$ residual was the most sensitive, with a $J(\theta) = 4.7857 \times 10^{-5}$.

The third order ARX parameter are collected in the parameter vector $\theta = [0.2018, -1.3242,$

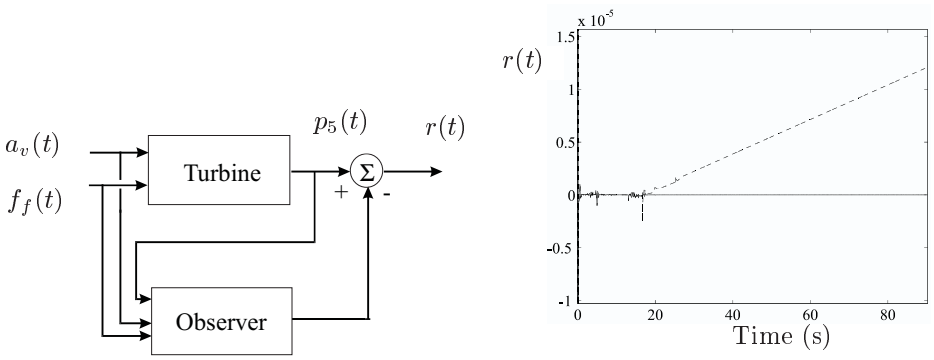


(a) $p_5(t)$ residual generation scheme (b) $p_5(t)$ observer residual

Figure 20: (a) $p_5(t)$ signal residuals and (b) observer scheme.

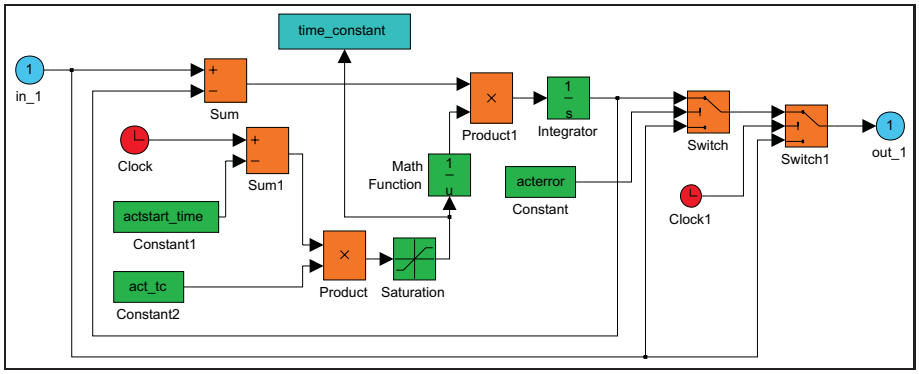


Figure 21: Actuator fault SIMULINK model.

2.1207, −0.0069, 0.0632, −0.0560, 0.0187, −0.0464, 0.0286].

In Figure (22(b)) is depicted the observer scheme used to generate residual regarding the signal $p_3(t)$. $a_v(t)$, $f_f(t)$ and $p_3(t)$ are the inputs of the output observer used to estimate the $p_3(t)$ signal itself.

Figure (23(a)) depicts the dynamics of the $p_3(t)$ signal, while the effects of the fault on the symptom signal $r(t)$ is shown in Figure (23(b)). $r(t)$ is the residual concerning the $p_3(t)$ output measurement in fault-free and faulty conditions. Because of the closed-loop configuration of the subsystem considered in Figure (22(b)), the fault shape can not be described by using a ramp function.

As depicted in Figure (22(a)) an output observer fed by inputs $a_v(t)$ and $f_f(t)$ was designed to estimate $p_3(t)$. The eigenvalues $\mathbf{p}$ were chosen near 0.4 to minimise the cost function $V(\mathbf{p})$.

In Figure (24), the function $V(\mathbf{p})$ is depicted, with $p_1 = \ldots p_{n-1} = 0.4$ and $\mathbf{p} \equiv p_n$.

Figure (25(b)) shows how the fault occurring on the single sensor causes alteration of the input and output signals and of the residuals given by the output observer using the $p_3(t)$ signal as input. These residuals indicate a fault occurrence when their values are lower or higher than the thresholds fixed in fault-free conditions.

Figure (25(b)) shows the fault-free (solid line) and faulty (dotted line) residual $r(t)$ obtained from the difference between the values computed by the observer related to the output $p_3(t)$ and the ones given by the sensor.

In order to improve the fault detection capabilities of the proposed method regarding the "case 4", another technique will be presented.

A *Kalman filter*, used as parameter estimator, has been exploited in order to detect changes in

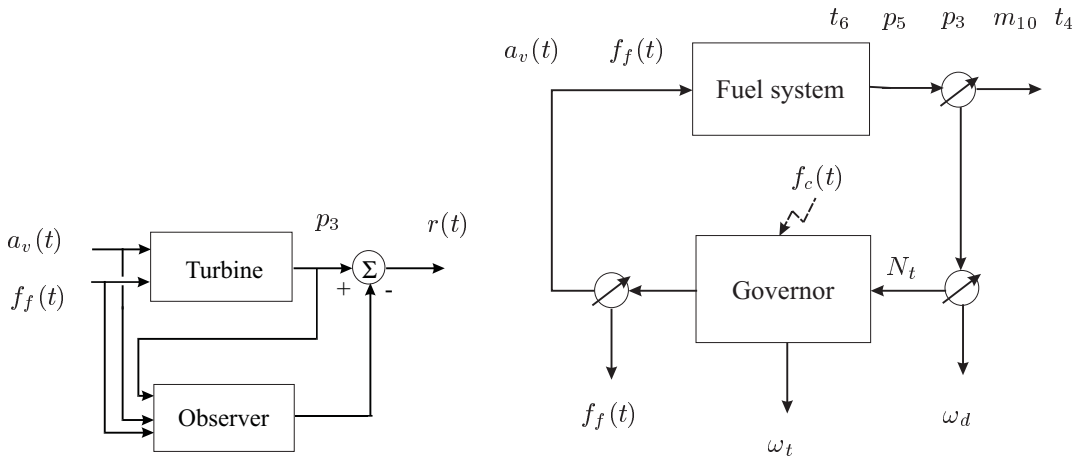


(a) The observer scheme

(b) The diagnosis subsystem

Figure 22: Schemes for the fuel actuator fault.

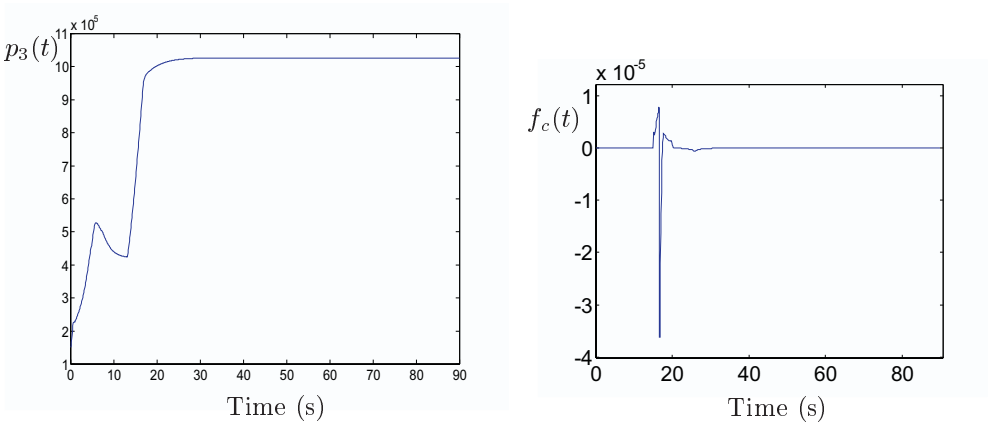


(a) The $p_3(t)$ signal.

(b) The fault $f_c(t)$ concerning $p_3(t)$

Figure 23: Diagnosis of the $p_3(t)$ signal

parameters due to output faults. The system has the form

$$\begin{cases} \theta(t+1) = \theta(t) + \omega(t) \\ y(t) = \mathbf{C}(t)\ \ \theta(t) + \varepsilon(t) \end{cases} \tag{36}$$

where $\theta(t)$ is the parameter vector, $\mathbf{C}(t) = [y(t-n), \ldots, y(t-1), u(t-n), \ldots, u(t-1)]$, the measurement vector, $n$ the order of the model, $\omega(t)$ a white process, in order to take into account the parameter variations for non stationary processes and $\varepsilon(t)$ the equation error term.

Figure (26(a)) depicts the recursive estimation of one entry of the parameter of the MISO ARX model for the $p_3(t)$ output given by the Kalman filter (solid line) and the estimate computed by the OLS (Ordinary Least Square) method (dotted line) [Ljung, 1999]. Note how the real process with $a_v(t)$ and $f_f(t)$ as inputs and $p_3(t)$ as output is non stationary and the estimates are different. Figure (26(b)) shows the change of the most sensitive parameter $\theta_i(t)$ of $\theta(t)$ due a fault, by using

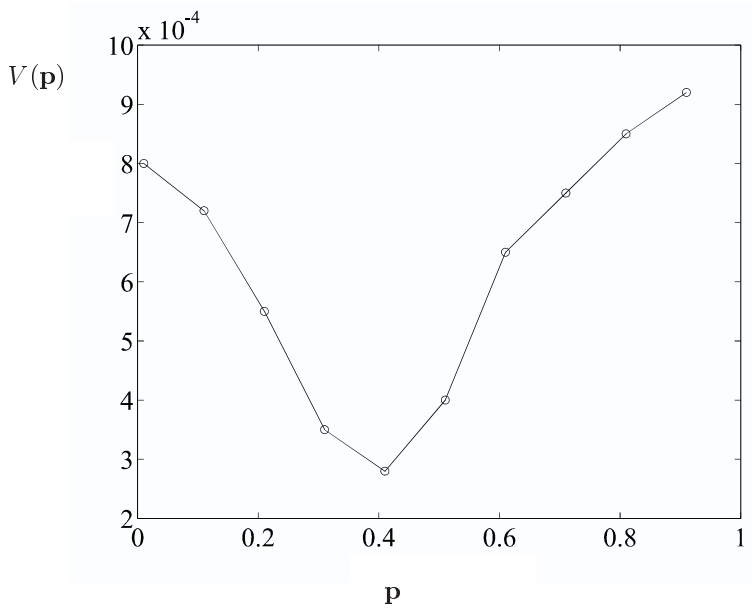


Figure 24: The cost function $V(\mathbf{p})$

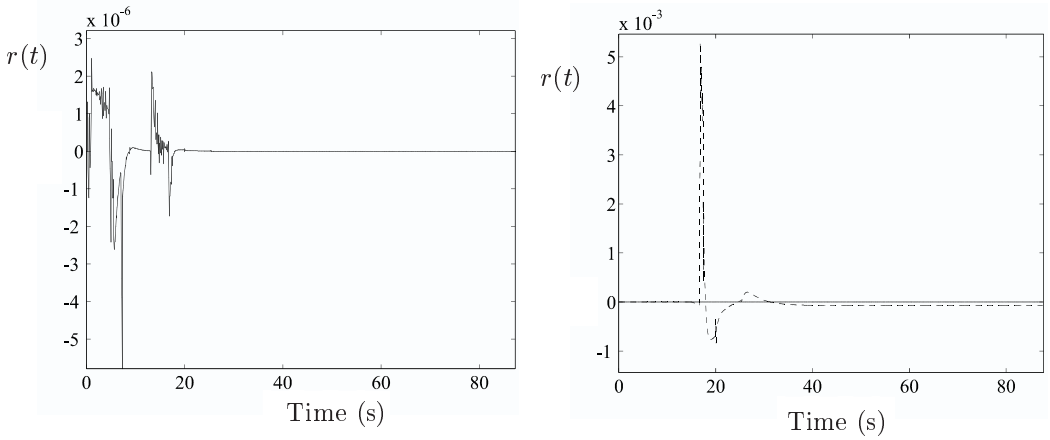


(a) Fault-free residual

(b) Residual in the presence of $f_c(t)$ fault

Figure 25: The fault free and faulty residual signals.

the Kalman filter for a third order ARX model ($n = 3$), with a covariance matrix for $\varepsilon(t)$ and $\omega(t)$ processes estimated from the OLS.

Even if the $f_c(t)$ actuator fault occurs as a ramp increase in the fuel valve constant time with $t \leq 0$ and since it is injected into the feedback controller system by means of non–linear links, the fault effects on output measurements are different from a ramp mode.

In particular, the "case 4" fault mode is depicted in Figure (23(b)) and the non–linear effect on $\theta_i(t)$ of the $f_c(t)$ signal is very similar to a step change, as shown in Figure (26(b)).

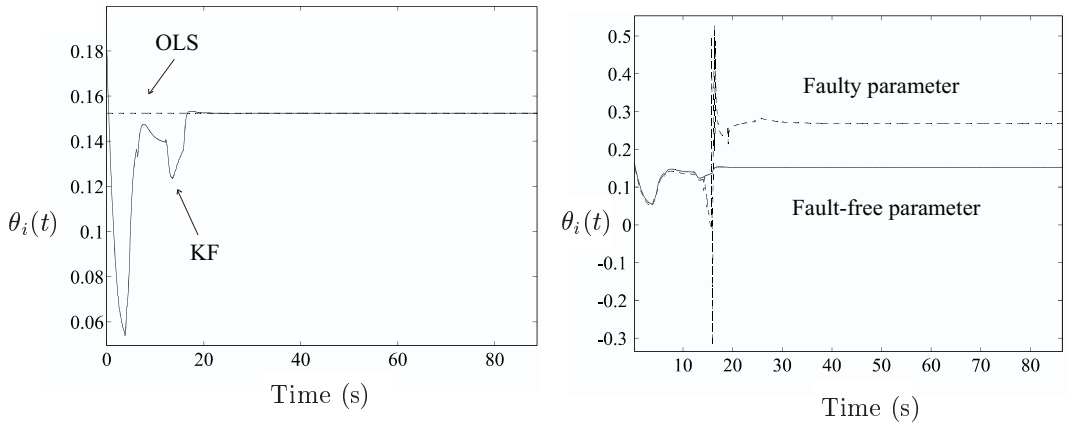


(a) $\theta_i(t)$ parameter variation due to a fault

(b) Fault free and faulty parameter

Figure 26: Kalman filter parameter variations due to the $f_c(t)$ fault.

# 9 Fault Isolability

By performing residual sensitivity analysis, i.e. by selecting the most sensitive residuals to the faults, the Table (4) is obtained, in order to isolate different fault occurring at the same time.

| Fault/$r(t)$ | $p_3$ | $p_4$ | $p_5$ | $p_7$ | $p_t$ | $q_a$ | $q_c$ | $q_f$ | $t_{3n}$ | $t_5$ | $t_6$ |
|---|---|---|---|---|---|---|---|---|---|---|---|
| Case 1 | **1** | **1** | **1** | 0 | 0 | 0 | *1* | 0 | 0 | 0 | 0 |
| Case 2 | 0 | 0 | 0 | 0 | 0 | 0 | 0 | 0 | *1* | 0 | 0 |
| Case 3 | **1** | **1** | **1** | *1* | **1** | 0 | 0 | 0 | 0 | *1* | *1* |
| Case 4 | **1** | **1** | **1** | 0 | **1** | *1* | 0 | *1* | 0 | 0 | 0 |

Table 4: Fault signature.

In order to summarise the FDI capabilities of the presented schemes, Table (4) shows the "fault signatures" in case of a single fault in each actuator, component and sensor. The residuals which are affected by faults are marked with the presence of '1' in the correspondent table entry, while an entry '0' means that the fault does not affect the correspondent residual.

The bold face entries in the table represent the residuals affected by the same faults. The italics '1's are the distinguishable residuals (they are bigger than a fixed threshold).

Note how multiple faults in actuator, components and sensor can be isolated since a fault affects only the residual function of the observer driven by the same output.

# 10 FDI in stochastic environment

In this section, a FDI technique based on Kalman filters designed in stochastic environment is presented [Simani and Spina, 1998, Simani et al., 2000a].

Such a design is enhanced by processing the noisy data according to the Frisch scheme identification method [Simani et al., 2000a].

Moreover, fault size estimation can be performed by means of different neural network architectures. In particular, neural networks can be used as function approximators to estimate single sensor fault size [Simani et al., 1998, Simani et al., 1999b].

The proposed fault diagnosis tool in stochastic environment is tested on the power plant presented in the previous sections.

## 10.1 Fault estimation device

The fault detection and diagnosis system produces and elaborates a set of residuals from which it will be possible to estimate the amplitudes of the faults regarding actuators, components and input-output sensors.

With reference to Figure (27) the symptom generator is designed to produce a set of signals which are somehow redundant. These signals are differences between estimated signals given by Kalman filters and the actual ones supplied by the sensors.

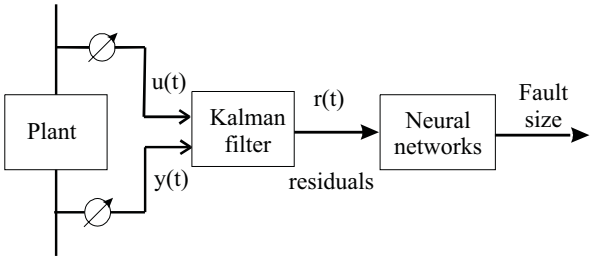


Figure 27: Logic diagram of the fault detection system.

In order to experiment with learning capabilities of artificial neural networks, on which the diagnosis device in Figure (27) is based, a bank of classic Kalman filters are used. The number of filters is equal to the number $m$ of system outputs, and each filter is driven by a single output measurement and all the inputs of the plant. Because of this configuration, the diagnosis of faults is indeed very easy, since each output measurement is directly connected to a single residual generator.

The basic principle of fault detection by using Kalman filtering is illustrated in Figure 28.

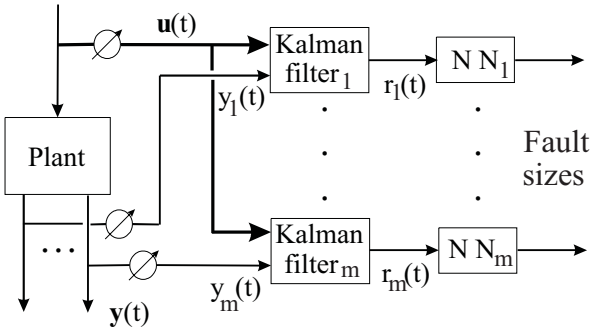


Figure 28: Bank of Kalman filters and NNs for residual generation and estimation.

With reference to the time-invariant, discrete-time, linear dynamic system described by a minimal state-space realisation $(\mathbf{A}_i, \mathbf{B}_i, \mathbf{C}_i)$ of the input-output MISO system (6) [Söderström and Stoica, 1987], the $i$-th Kalman filter has the structure [Jazwinski, 1970]:

$$\begin{cases} \mathbf{x}^i(t+1|t) = \mathbf{A}_i \left(\mathbf{I} - \mathbf{K}_i(t)\mathbf{C}_i\right) \mathbf{x}^i(t|t-1) + \mathbf{B}_i\mathbf{u}(t) + \mathbf{A}_i\mathbf{K}_i(t)y_i(t) \\ y^i(t|t) = \mathbf{C}_i \left(\mathbf{I} - \mathbf{K}_i(t)\mathbf{C}_i\right) \mathbf{x}^i(t|t-1)\mathbf{C}_i\mathbf{K}_i(t)y_i(t) \end{cases} \tag{37}$$

The variable $\mathbf{x}^i(t+1|t)$ is the one step ahead prediction of the state $\mathbf{x}_i(t)$, $y^i(t|t)$ is the estimate of the $i$-th component $y_i(t)$ of the output $\mathbf{y}(t)$ given by the filter.

A Riccati equation is used to compute the time-variant gain $\mathbf{K}_i$ of the filter by means of the knowledge of the covariance matrix of the input vector noise $\tilde{\mathbf{u}}(t)$ and the variance of the $i$-th component of the output noise $\tilde{\mathbf{y}}(t)$.

It can be proved that the innovation $r_i(t+1) = y_i(t+1) - \mathbf{C}_i\mathbf{x}^i(t+1|t)$ is a white process when all the assumptions regarding the system $(\mathbf{A}_i, \mathbf{B}_i, \mathbf{C}_i)$ and the statistical characteristics of the noises are completely fulfilled. In particular, the innovation converges to a steady state solution when the pair $(\mathbf{A}_i, \mathbf{B}_i)$ is completely observable and the pair $(\mathbf{A}_i, \mathbf{C}_i)$ is completely reachable.

## 10.2 Identification procedure

The Frisch scheme can be applied to perform the dynamic system identification of the plant [Frisch, 1934, Kalman, 1982, Kalman, 1990, Beghelli et al., 1990, Beghelli and Soverini, 1992].

Such a scheme permits to determine the linear discrete dynamic system which has generated the noisy sequences as well as the variances of the noises $\tilde{\mathbf{u}}(t)$ and $\tilde{\mathbf{y}}(t)$ corrupting the data.

In the Frisch scheme these signals are assumed white noises, mutually uncorrelated and uncorrelated with every component of $\mathbf{u}^*(t)$ and $\mathbf{y}^*(t)$.

The Table (5) summarises the reconstruction errors concerning the MISO models in the form (17) with two inputs ($a_v(t)$ and $f_f(t)$) and each monitored output variable, as output.

| Variable | Name | Model order | $J(\theta)$ | Accuracy | Ref. |
|---|---|---|---|---|---|
| $p_5$ | Pressure | 2 | 0.0054 | 1% | 940014.006 |
| $p_3$ | Pressure | 2 | 0.0049 | 1% | 1026228.8381 |
| $q_c$ | Torque | 2 | 0.0042 | $\pm$ 5 % | 3144.1183 |
| $t_{3n}$ | Temperature | 2 | 0.0031 | $1.5^o$ | 578.5759 |

Table 5: Frisch scheme model reconstruction errors.

Table 6 collects parameters of second order models ($n = 2$) as well as the input and output noises.

| Variable | Model parameters $\theta$ | Input noises $\tilde{\sigma}_u$ | Output noise $\tilde{\sigma}_y$ |
|---|---|---|---|
| $p_5$ | [−0.0295, 1.0054, 0.1369, −0.1328, 0.0402, −0.0232] | [0.0004, 0.0023] | 0.0026 |
| $p_3$ | [0.6655, 0.2885, −0.0579, 0.0651, 0.2408, −0.2065] | [0.0004, 0.0023] | 0.0026 |
| $q_c$ | [−0.9920, 1.9904, −0.0179, 0.0181, 0.0111, −0.0100] | [0.0004, 0.0023] | 0.0015 |
| $t_{3n}$ | [−1.1760, 2.1882, 0.0283, −0.0311, −0.3202, 0.3133] | [0.0004, 0.0023] | 0.0024 |

Table 6: Frisch 2-nd order model parameters and noise variances.

On the basis of the data collected in Table (6), four Kalman filters with two inputs ($r = 2$) and one output ($m = 1$) were designed.

The detection strategy which is commonly chosen in connection with Kalman filtering methods for failures detection, consists in monitoring the innovations $r(t)$.

Because of the linear property of system (1) and because of the effect of faults on the system output measurements, any change in measurements due to a fault is reflected in a change in the mean and in the standard deviation of $r(t)$.

In particular, since the Kalman filter produces zero-mean and independent white residuals with the system in normal operation, a method for failure detection and isolation consists in testing how much the sequence of innovations has deviated from the white noise hypothesis. The tests which can be performed on the innovations are the usual ones for zero-mean and variance, as cumulative sum algorithms as well as independence, as $\chi^2$-type.

If a system abnormality occurs, the statistics of $r(t)$ change, so its comparison with a threshold fixed under no faults conditions, becomes the detection rule.

In Figures (29), (30), (31) and (32) the examples of the turbine FDI performed by using the residual generated by the Kalman filter with two inputs and one output are shown.

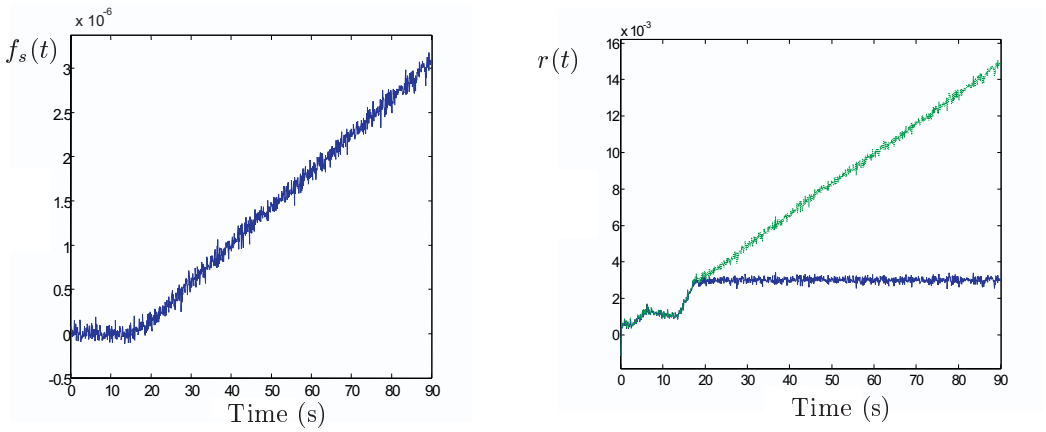


(a) System fault $f_s(t)$

(b) "Case 1" residual

Figure 29: (a) Component fault "case 1" and (b) Kalman filter residual.

In particular, Figure (29(a)) shows the value of the fault $f_s(t)$ affecting the $q_c(t)$ residual ("case 1"), whilst Figure (29(b)) depicts fault-free and faulty residuals generated by the Kalman filter.

It is driven by the input sensor signal $a_v(t)$, $f_f(t)$ and the $q_c(t)$ signal itself. A ramped incipient compressor fault ("case 1"), commencing at $t = 15$s causes a change in the value of the $q_c(t)$ residual computed in fault-free condition, as depicted in Figure (29(b)).

It is important to note that, in order to achieve the maximal fault detection capability, the residual corresponding to the most sensitive filter to a failure on the $q_c(t)$ measurement was selected, in accordance with Table (5).

Figure (30(a)) shows the value of the $f_y(t)$ incipient ramp fault ("case 2") affecting the output sensor for the measurement of the $t_{3n}$ signal and commencing at the instant $t = 15$ sec.

In Figure (30(b)) fault free and faulty residuals regarding the $t_{3n}$ signal obtained from the difference between the values $y^i(t|t)$ computed by the Kalman filter in Equations (37) with $t_{3n}$ and the ones measured by the sensor, are shown.

Obviously, the non-zero value of the residual in fault-free conditions is due to the ARX model approximation and to the actual measurement noise.

Figure (31(b)) shows the behaviour of the residual when a ramped incipient fault $f_s(t)$ ("case 3") commences at the instant $t = 15$ sec.

The $f_s(t)$ fault mode is depicted in Figure (31(a)).

According to Table (5), in this case, $p_5(t)$ is the monitored signal for the FDI of a component of the turbine.

Figure (31(b)) depicts the fault-free residual and its change due to the fault occurrence, as the previous cases.

Finally, Figure (32(b)) shows the change in the fault-free residual concerning the $y_i(t) = q_t(t)$ measurement due to a ramped incipient actuator fault ("case 4").

The $f_c(t)$ fault commences at the instant $t = 15$ sec. The fault mode is depicted in Figure (32(a)).

In Figure (32(b)) on the right the fault-free and the faulty residuals are shown.

Because the nature of the incipient ramp fault $f_c(t)$ affecting the regulator into the feedback control loop, the output measurements affected by the fault itself are different from ramp signals, as depicted in Figure (32(a)).

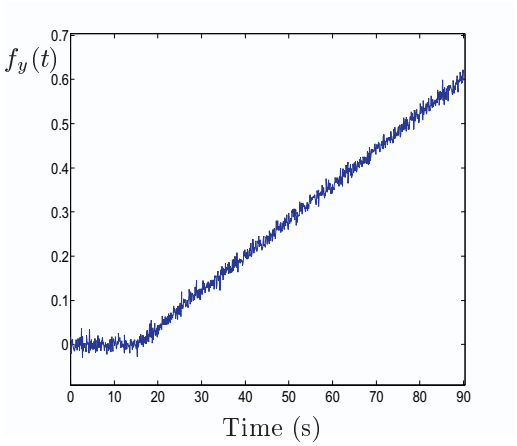


(a) Output sensor fault $f_y(t)$

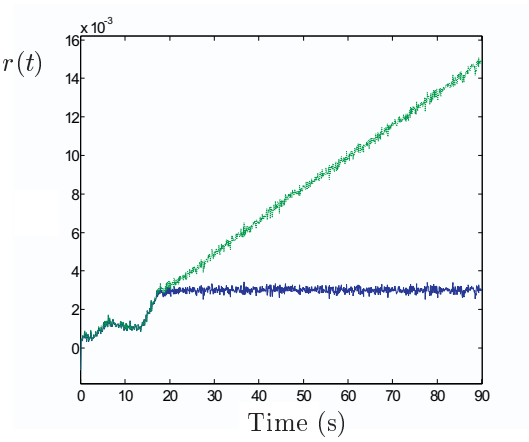


(b) $r(t)$ "Case 2" residual

Figure 30: (a) Output ("case 2") sensor fault and (b) Kalman filter residuals.

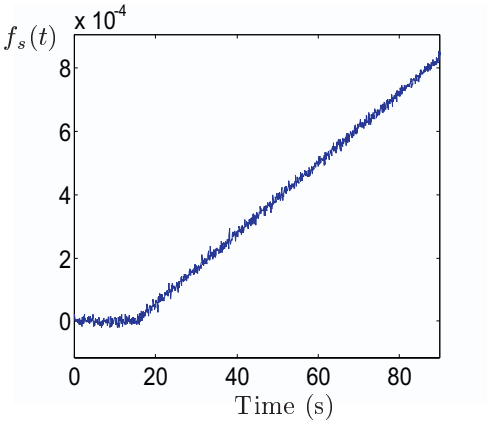


(a) System fault $f_s(t)$

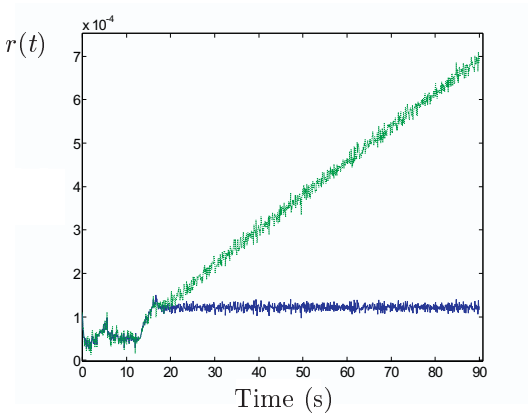


(b) $r(t)$ "Case 3" residual

Figure 31: (a) Component ("case 3") fault and (b) Kalman filter residuals.

# 11 Minimal detectable faults

Table (7) summarises the performance of the fault detection and isolation technique both in the deterministic and stochastic environment.

The Table collect the minimal detectable fault on the four measurements, in case the residual or innovation value is monitored using a geometrical test and fixed thresholds.

The minimal detectable fault values in Table 7 are expressed as percentage of the signal values and are relative to the case in which the occurrence of a fault must be detected as soon as possible. It results that the values of the faults obtained by using geometrical analysis on Kalman filter innovations, collected in Table 7, are different than the ones reported in the same Table and computed in the deterministic environment exploiting classical observers.

Table 7 shows how faults modeled by ramp functions may not be immediately detected, since the delay in the corresponding alarm normally depends on fault mode.

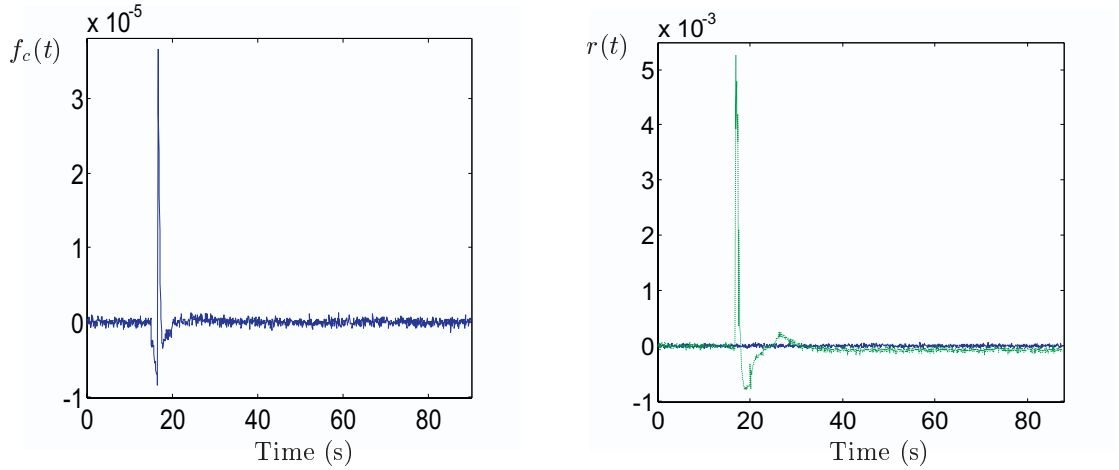


(a) Actuator fault $f_c(t)$

(b) $r(t)$ "Case 4" residual

Figure 32: (a) Actuator fault ("case 4") and (b) Kalman filter residuals.

| Fault Case | Monitored signal | Deterministic environment | Stochastic environment | Detection delay |
|---|---|---|---|---|
| Case 1 (Compressor contamination) | $q_c(t)$ | 0.5% | 1% | 30s |
| Case 2 (Thermocouple sensor fault) | $t_{3n}(t)$ | 10% | 12% | 30s |
| Case 3 (Turbine seal damage) | $p_5(t)$ | 5% | 7% | 60s |
| Case 4 (Fuel actuator fault) | $p_3(t)$ | 1% | 3% | 10s |

Table 7: Minimum detectable faults by monitoring residual and innovation values.

The minimal detectable fault can be found by fixing a detection delay, defined in Figure (33). If a delay in detection is tolerable the amplitude of the minimal detectable fault is lower.

The minimal detectable faults on the various sensors seem to be adequate to the industrial diagnostic applications, by considering also that the minimal detectable faults can be reduced if a delay in detection promptness is tolerable.

# 12 Fault diagnosis neural networks

In recent years, neural networks have been exploited successfully in pattern recognition as well as function approximation theory and they have been proposed as a possible technique for fault diagnosis, too. Neural networks can handle non-linear behaviour and partially known process.

The aim of this paragraph is to suggest how artificial neural networks can be exploited to approximate a large class of functions, for fault diagnosis of an industrial plant.

In particular, the problem of the estimate of the slope of faults concerning actuators, components and output sensors of an industrial gas turbine can be solved. Faults modeled by ramp functions create changes in several residuals obtained by using dynamic observers (Kalman filters) of the process under examination.

A neural network can be used in order to find the connection from a particular fault regarding input and output sensors to a particular residual. Residuals are dependent only on sensors faults. Therefore, the neural network evaluates patterns of residuals, uniquely related to particular fault conditions [Simani et al., 1998, Simani et al., 1999b].

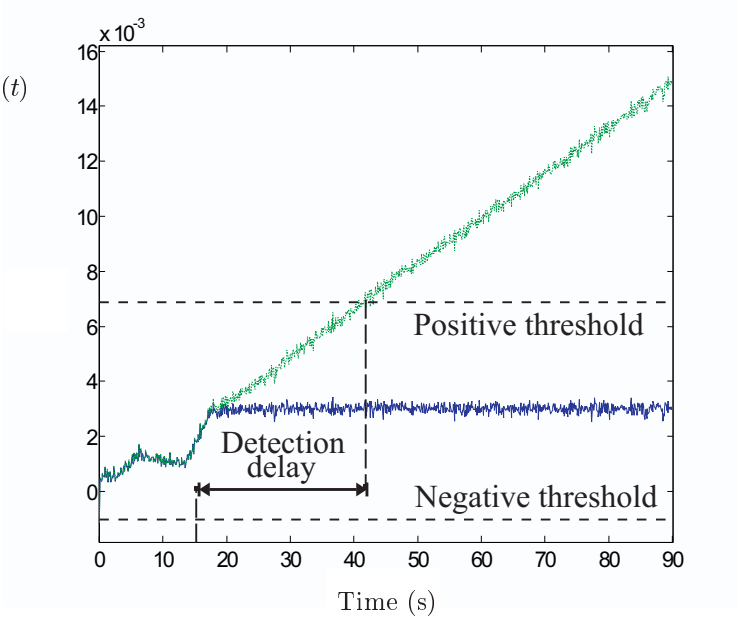


Figure 33: Detection delay definition.

# 13 Conclusions and future works

The complete design procedure for FDI in actuators, components and output sensors of an industrial process was described in this report.

The fault diagnosis was performed by using a bank of dynamic observers or, when the measurement noises are not negligible, a bank of Kalman filters. Single fault on the component of the system, actuator and output sensors were therefore considered

The suggested method did not require any physical knowledge of the process under observation since the input-output links were obtained by means of an identification scheme, which uses ARX models in case of high signal to noise ratios or errors-in-variables models, otherwise. In last situation the identification technique (Frisch scheme) gave the variances of the input-output noises, which are required in the design of the Kalman filters.

Such a procedure was applied to a SIMULINK© model of a single-shaft industrial gas turbine. In order to analyse the diagnostic effectiveness of the FDI system in the presence of changes or drifts in measurements, faults modeled by ramp functions were generated.

The results obtained by this approach indicated that the minimal detectable faults on the system actuator, component and output sensor are of interest for the industrial diagnostic applications.

However, since in real industrial applications incipient ramp faults develop slowly over a long period, in order to avoid excessively long duration simulations, the fault development rate was increased so that significant effects were present after shorter periods. This is a factor which must be taken account for the FDI performance evaluation.

The main aspect of this work was the use of linear system identification and modeling methods, although the system considered was non–linear. This is considered important to avoid the complexities that would otherwise be inevitable when non–linear models are used. There is certainly an increasing interest in the use of non–linear methods (non–linear observers, extended Kalman filters, fuzzy-logic methods, etc). By the same authors, see for example [Chen and Patton, 1999, Simani, 1999b, Simani, 1999a, Simani et al., 2000c, Simani et al., 2000b, Simani, 2000].

However, as the feature of system supervision is to monitor the operation and performance of the system with respect to an expected point of operation, linear system methods are still very valid. Deviations from expected behaviour can be used to monitor system performance changes as well as system component malfunctions.

Finally, simulation results showed that the minimal detectable fault sizes, obtained by using geometrical analysis of Kalman filter innovations, are smaller than the ones computed in the deterministic environment and exploiting classical Luenberger observers. Moreover, if a delay in detection is tolerable the amplitude of the minimal detectable fault is lower.

The minimal detectable faults on the various sensors seem to be adequate to the industrial diagnostic applications, by considering also that the minimal detectable faults can be reduced if a delay in detection promptness is tolerable.

# References


[Baseville, 1988] Baseville, M. (1988). Detecting changes in signal and systems: A survey. *Automatica*, 24:309–326.

[Beghelli et al., 1994] Beghelli, S., Castaldi, P., Guidorzi, R. P., and Soverini, U. (1994). A comparison between different model selection criteria in Frisch scheme identification. *Systems Science Journal*, 20(1):77–84. Wroclaw, Polonia.

[Beghelli et al., 1990] Beghelli, S., Guidorzi, R. P., and Soverini, U. (1990). The Frisch scheme in dynamic system identification. *Automatica*, 26(1):171–176.

[Beghelli and Soverini, 1992] Beghelli, S. and Soverini, U. (1992). Identification of linear relations from noisy data: Geometrical aspects. *System and Control Letters*, 18(5):339–346.

[Chen and Patton, 1999] Chen, J. and Patton, R. J. (1999). *Robust Model-Based Fault Diagnosis for Dynamic Systems.* Kluwer Academic Publisher.

[Frank, 1990] Frank, P. M. (1990). Fault diagnosis in dynamic systems using analytical and knowledge-based redundancy: A survey and some new results. *Automatica*, 26.

[Frank and Ding, 1997] Frank, P. M. and Ding, X. (1997). Survey of robust residual generation and evaluation methods in observer-based fault detection system. *J. Proc. Cont.*, 7(6):403–424.

[Frisch, 1934] Frisch, R. (1934). *Statistical Confluenece Analysis by Means of Complete Regression Systems.* University of Oslo, Economic Institute, publication n. 5 edition.

[Gertler, 1998] Gertler, J. (1998). *Fault Detection and Diagnosis in Engineering Systems.* Marcel Dekker, New York.

[Guidorzi and Rossi, 1974] Guidorzi, R. P. and Rossi, R. (1974). Identification of a power plant from normal operating records. *Automatic Comtrol Theory and Applications*, 2(3):63–67.

[Isermann, 1984] Isermann, R. (1984). Process fault detection based on modelling and estimation methods: A survey. *Automatica*, 20.

[Isermann and Ballé, 1997] Isermann, R. and Ballé, P. (1997). Trends in the application of model-based fault detection and diagnosis of technical processes. *Control Engineering Practice*, 5(5):709–719.

[Jazwinski, 1970] Jazwinski, A. H. (1970). *Stochastic processes and filtering theory.* Academic Press, New York.

[Kalman, 1982] Kalman, R. E. (1982). System identification from noisy data. In Bednarek, A. and Cesari, L., editors, *Dynamical System II*, pages 135–164. Academic Press, New York.

[Kalman, 1990] Kalman, R. E. ((Springer-Verlag, Berlin, 1990)). Nine lectures on identification. *Lecture Notes on Economics and Mathematical System.*

[Leontaritis and Billings, 1985] Leontaritis, I. J. and Billings, S. A. (1985). Input-output parametric models for non-linear systems. *Int. J. Control*, 41:303–344.

[Ljung, 1999] Ljung, L. (1999). *System Identification: Theory for the User*. Prentice Hall, Englewood Cliffs, N.J., second edition.

[MathWorks, 1992] MathWorks (1992). *SIMULINK: User's Guide*. The MathWorks Inc., Natick, Mass.

[Patton, 1996] Patton, R. J. (1996). Design of unknown input observers and robust fault detection filters. *Int. J. Control*, 63(1):95–105.

[Patton et al., 1989] Patton, R. J., Frank, P. M., and Clark, R. N. (1989). *Fault Diagnosis in Dynamic Systems, Theory and Application*. Control Engineering Series. New York: Prentice Hall, Hertfordshire.

[Simani, 1999a] Simani, S. (1999a). Fuzzy multiple inference identification and its application to fault diagnosis of industrial processes. In *ISAS'99/SCI'99*, volume 7, pages 185–191, Orlando, FL, USA. The Fifth Conference of the ISAS (Information Systems Analysis and Synthesis)/ The Third Conference of the SCI (Systemics, Cybernetics and Informatics).

[Simani, 1999b] Simani, S. (1999b). Sensor fault diagnosis of a power plant: an approach based on state estimation techniques. In Mastorakis, N. E., editor, *IMACS-IEEE'99*, volume Recent Advances in Signal Processing and Communications, pages 274–281, Athens. International Conference on Computer Engineering in System Applications, World Scientific Engineering Society.

[Simani, 2000] Simani, S. (2000). *Model-based fault diagnosis in dinamic systems using identification techniques*. PhD thesis, Department of Engineering, University of Ferrara.

[Simani et al., 1999a] Simani, S., Fantuzzi, C., and Beghelli, S. (1999a). Improved observer for sensor fault diagnosis of a power plant. In *MED99. The 7th IEEE Mediterranean Conference on Control & Automation*, pages 826–834, Haifa, Israel.

[Simani et al., 2000a] Simani, S., Fantuzzi, C., and Beghelli, S. (2000a). Diagnosis techniques for sensor faults of indistrial processes. *IEEE Transactions on Control Systems Technology*. (To appear).

[Simani et al., 2000b] Simani, S., Fantuzzi, C., Beghelli, S., and Rovatti, R. (2000b). Identification of hybrid model in noisy environment. *International Journal of Control*. (Submitted).

[Simani et al., 2000c] Simani, S., Fantuzzi, C., Rovatti, R., and Beghelli, S. (2000c). Nonlinear dynamic system modelling in noisy environment using multiple model approach. In *ACC'00*, Chicago, Illinois, USA. American Control Conference. (Accepted).

[Simani et al., 1998] Simani, S., Fantuzzi, C., and Spina, P. R. (1998). Application of a neural network in gas turbine control sensor fault detection. In *CCA'98*, Trieste, Italy. 1998 IEEE Conference on Control Applications.

[Simani et al., 1999b] Simani, S., Marangon, F., and Fantuzzi, C. (1999b). Fault diagnosis in a power plant using artificial neural networks: analysis and comparison. In *ECC'99*, Karlsruhe, Germany. European Control Conference 1999.

[Simani and Spina, 1998] Simani, S. and Spina, P. R. (1998). Kalman filtering to enhance the gas turbine control sensor fault detection. In *6th IEEE Med '98*, Alghero, Sardinia, Italy. The 6th IEEE Mediterranean Conference on Control and Automation.

[Söderström and Stoica, 1987] Söderström, T. and Stoica, P. (1987). *System Identification*. Prentice Hall, Englewood Cliffs, N.J.

[Willsky, 1976] Willsky, A. S. (1976). A survey of desogn methods for failure detection systems. *Automatica*, 12.

[Xie and Soh, 1994] Xie, L. and Soh, Y. C. (1994). Robust Kalman filtering for uncertain systems. *Systems and Control Letters*, 22:123–129.

[Xie et al., 1994] Xie, L., Soh, Y. C., and de Souza, C. E. (1994). Robust Kalman filtering for uncertain discrete-time systems. *IEEE Transaction on Automatic Control*, 39:1310–1314.